Lappeenranta University of Technology

School of Engineering Science

Degree Program in Chemical and Process Engineering

Master's Thesis – Lappeenranta, 2018

Shahla Huseynova

Determination of particle size distributions of industrial side streams by using laser diffraction and sieving methods

Examiner: Professor Antti Häkkinen

Supervisor: D.Sc. (Tech.) Teemu Kinnarinen

Abstract

Lappeenranta University of Technology
LUT School of Engineering Science
Degree Program in Chemical and Process Engineering

Shahla Huseynova

Determination of particle size distributions of industrial side streams by using laser diffraction and sieving methods

Master's thesis

2018

71 pages, 30 figures, 6 tables and 3 appendices

Examiners: Professor Antti Häkkinen
D.Sc. (Tech.) Teemu Kinnarinen

Keywords: particle size distribution, industrial solid side streams, laser diffraction, sieving

Due to high transportation and treatment costs, the disposal of industrial solid residues has been preferred for backfilling mine openings over years. Recently, utilization of such residues has gained an increasing interest in different areas, especially as a supplementary cementitious material in concrete industry. Achieving this will also contribute to building long-term sustainable method to decrease GHG emission.

The aim of this work was to measure particle size distribution (PSD) of the materials as it plays a key importance in the product quality. For this purpose, different PSD determination and classification techniques were studied, and laser diffraction and sieving methods were decided to use. The samples to be analyzed were ashes, green liquor dregs, tailings, lime mud consisting mainly of $CaCO_3$, coating sludge, deinking flotation reject foam, lime and construction waste. LD and sieving measurements were performed with Malvern Mastersizer 3000 and Haver & Boecker sieve shaker, respectively. It was found that ash samples, construction waste and tailings gave good correlation between two methods while lime samples (# 3, 12, 13) had poor correlation. Deviation between results happened mostly when the particles were elongated, rods, irregular shaped and sticky. Moreover, it was observed that the results are more reliable when the combination of these methods was used, especially for the samples that have non-uniform particle population.

Acknowledgements

I would like to thank LUT and all the faculty, staff and support services for providing such amazing opportunities and a welcoming study environment that have raised my awareness towards sustainability and enabled me to bring my degree to a completion. I am so grateful for that well-rounded education.

A special thanks to Professor Antti Häkkinen for introducing me with this interesting research topic. It was an honor and great opportunity for me to work under his supervision.

My heartfelt gratitude goes to D.Sc Teemu Kinnarinen for advising me during this research project. His valuable insights, support and guidance helped me not to stray from the main idea of the thesis and gave me chance to work independently.

I also owe my sincere thanks to Laboratory Technician Toni Väkiparta for giving instructions on how to handle the Mastersizer 3000 analyzer and answering all my questions.

I would be remiss if I didn't thank my family, my friends back home and my cousins, especially Nigar Aliyeva for being always there for me through thick and thin. I am also appreciative for the friends I have met here and for the friendships that will hopefully last forever, over national borders and continents. Thank you! Kiitos! Təşəkkürlər!

To my father, my inspirer and anchor Yagub Huseynov

Shahla Huseynova

Lappeenranta, September 2018

This thesis has been supported by the Urban Innovative Actions Initiative

TABLE OF CONTENTS

LIST OF FIGURES

LIST OF TABLES

List of symbols and abbreviations

A	projected surface area	m^2
C_D	drag coefficient	-
d	particle diameter	m
D_A	equivalent circular area diameter	m
D_c	characteristic diameter of the unit	m
D_p	equivalent circular perimeter diameter	m
E_t	Ecart Terra index	-
F_D	drag force	$kg \cdot m/s^2$
F_{max}	maximum Feret diameter	m
I	imperfection index	-
L	particle length	m
$\dot{m}$	mass flow	kg/s
$\dot{m}_c$	mass flow of coarse particles	kg/s
$\dot{m}_f$	mass flow of fine particles	kg/s
$\dot{m}_0$	mass flow of the feed	kg/s
n	dimensionless uniformity index	-
P	perimeter of the particle	m
q_{ci}	particle size frequency of coarse particles	-
q_{fi}	particle size frequency of fine particles	-
q_{0i}	particle size frequency of the feed	-
R	particle radius	m
Re	Reynolds number	-
S	sphericity (2D)	-

Stk_{50}	Stokes number	-
u	fluid-particle relative velocity	m/s
u_t	terminal velocity	m/s
v	superficial characteristic velocity	m/s
v_r	radial settling velocity	m/s
W	particle width	m
x	size	m
x_g	geometric mean of distribution	m
X_R	position parameter	-
x_{50}, d_{50}	cut size	m
y	actual mass fraction in underflow	-
y'	corrected mass fraction	-
κ	sharpness index	-
μ	fluid dynamic viscosity	Pa·s
ρ	fluid density	kg/m^3
σ_g	geometric standard deviation	m
ψ	sphericity (3D)	-
ω	angular velocity	rad/san
GHG	greenhouse gas emission	
LD	laser diffraction	
OPC	ordinary portland cement	
PSD	particle size distribution	
SEM	scanning electron microscope	
TEM	transmission electron microscope	
US	ultrasound	

Introduction

The disposal and treatment of hazardous solid wastes of industries have been heretofore significant problems for the industries since it is a costly method to transport them to long distance and to treat. Such wastes are mostly used for backfilling mines and land areas. Particularly, hazardous sludges require a secure chemical landfill. Accumulated solid wastes may have harmful effects on surrounding living organisms and they cause the pollution. Since the increasing environmental pollution and greenhouse gas (GHG) emissions have become the major issue in this era, finding environmentally friendly solutions to sustain greener environment is now a global concern. (Badur & Chaudhary, 2008)

In recent years, it has attracted a worldwide research interest to recycle the industrial solid residues and byproducts and utilize them in the construction sites as supplementary cementitious materials which will decrease the dependency on cement in concrete industry. Concrete is a mixture of cementitious paste and aggregates. The paste (water and cement) is bound together with sands or aggregates where it gains strength and hardens through hydration reactions to form conglomerate stone, so-called concrete. Along with the binding properties of cement, concrete gains high strength and durability which makes it indispensable material in construction. (Badur & Chaudhary, 2008)

As a cementing material for concrete, Ordinary Portland cement (OPC) is a widely used type and its amount in concrete mix ranges between 10% and 15% by volume. Concrete consumption is in the first place on Earth among other man-made materials and its use is anticipated to increase significantly (Berry, et al., 2009). The amount of global cement production has been 5.07 billion metric tons in 2016 and it keeps growing by 2.5% annually (Edwards, 2017). In fact, the production of cement is not environmentally friendly, it has 7% share in worldwide GHG emissions; only CO_2 emission accounts for 1 ton per a ton of cement production (Abdulmatin, et al., 2017).

The aim of the industries is to build long-term sustainable method to decrease CO_2 emission in cement industry by replacing considerable amount of OPC and natural aggregates with the use of environmentally friendly materials. In addition, utilization of such industrial wastes will decrease the quantity of landfill wastes. These industrial wastes or by-products may include slag, clay, ash and sludge. Fly ash, byproduct from the combustion of coal, is one of the most chemically and physically potential materials to partly replace Portland cement whose production is 71 million tons per year nationwide in the US. In recent years, it has

been of great research interest to replace 100% of Portland cement with fly ash by maximum utilization of cementitious binding capacity of fly ashes (Berry, et al., 2009). The recycle process will also decrease the environmental pollution resulting from fly ash emission. According to Fisher et al. (1978), the amount of fly ash emitted from USA coal-fired electric plants to the atmosphere was estimated to be 2.4 million tons in 1974 when the collection efficiency of electrostatic precipitators for smaller particles was low. Therefore, fly ash emission has been very hazardous for human health as its atmospheric residence time is long and it is a potential hazard for ultimate human inhalation in case of the particles' being in the "respirable" size range. Recent years, there has been strict limitation for fly ash emission into atmosphere, especially in the countries where coal is the main energy source for power generation. Burning of coal emits hazardous fine particulates, such as SO_2, NO_x and some radioactive elements. (Zhang, 2016)

The researches show that biomass ash and other industrial side streams have biggest opportunities to be utilized in construction field, especially in cement and concrete products. Beside this, there are other potential utilization directions available, such as fertilizer applications and utilization in the production of ceramics and glasses and in asphalt/petroleum-based products. Green liquor dregs are also industrial side streams that has utilization areas. It is obtained mostly from kraft pulp processing and it can be utilized in the acidic wastewater treatment as a neutralizing agent. Lime, $CaCO_3$, slaked lime and tailings streams from carbonate mine are other potential solid residues which can also be further used in construction materials and in wastewater treatment. (Mäkitalo, et al., 2014)

The aim of the literature part of this thesis is to give comprehensive information behind the particle classification phenomenon and size and shape determination techniques of potential solid residues. Samples need to be analyzed in terms of their mechanical properties, durability, chemical properties and microstructure to ensure their suitability for replacing cement in geopolymer concrete production or in other utilization areas. However, this work has only focused on determination of particle size distribution of the samples and its measuring techniques. For this reason, detailed background information has been given about the classification methods, types of classifiers, particle properties and the analysis techniques of particle shape and size distribution.

I Literature part

1 Basis of classification

Classification is employed to separate particles into their fractions either from liquid or gas streams. It is a sorting method of particles according to their physical properties, such as their density, size and shape which gives different velocities to particles moving in fluid under a certain force. With this method, fine particles are separated from coarse ones and lighter particles from heavier ones. (Heiskanen, 1987)

A classifier is usually a complex system since several forces are involved in determining particles trajectories. Particles are accelerated externally by gravitation or centrifugal forces in the fluid where the fluid is usually water or air. Under the influence of these forces, particles start to move. The forces that act upon a particle are external force, buoyancy force which is an upward force that opposes the weight of the immersed object and the drag force. Drag force is a force that acts opposite to the particle motion in the suspension with respect to the fluid. When particles start accelerating they encounter an increasing resistance of the fluid due to drag and buoyancy forces. When the accelerating and resistance forces are equal, the settling particle reaches its maximum velocity which is called terminal velocity. Depending on differences in specific gravity and other properties of particles, terminal velocity varies. While large and dense particles possess higher settling velocities, small and light particles move with lower velocities and separation of size classes is achieved. (Cohen, 2012)

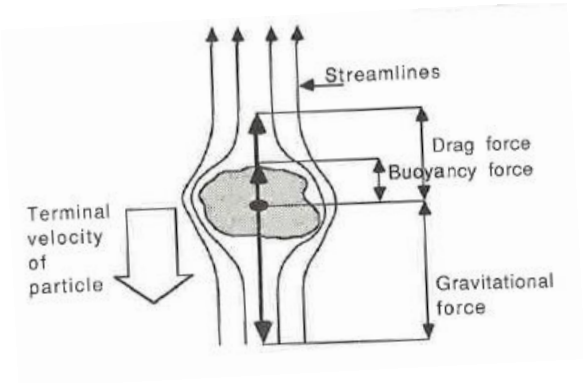

Figure 1. Acting of the balance of forces on a particle and streamlines of flow. (Heiskanen, 1987)

Streamlines are not being smooth if there is high velocity. Moreover, eddies form behind the particles because of fluid velocity and inertia. These eddies are called turbulence.

According to Ortega-Rivas (2012), it is necessary to know the magnitude of drag force in order to study the particle motion. The general expression of drag force, F_D is as follows:

$$F_D = C_D A \frac{\rho u^2}{2} \quad (1)$$

Where C_D drag coefficient

u fluid-particle relative velocity

A projected surface area

If the drag force is assumed to arise from fluid inertia, C_D will be constant. Drag coefficient is a dimensionless number and it is expressed as a function of particle Reynolds number (Eq. 2) which is also a dimensionless number.

$$Re = \frac{ud\rho}{\mu} \quad (2)$$

where d particle diameter

u terminal velocity

ρ fluid density

μ fluid dynamic viscosity

The Reynolds number is used to determine different flow regimes of the system which are (Heiskanen, 1987):

- Laminar regime – when Re < 0.2
- Transitional regime – when 0.2 < Re < 1000
- Turbulent regime – when Re > 1000.

In classification, it is often assumed that particles are spherical as the calculation of spheres is theoretically the most feasible. The function of drag force changes depending on the flow regime as presented in Fig. 2.

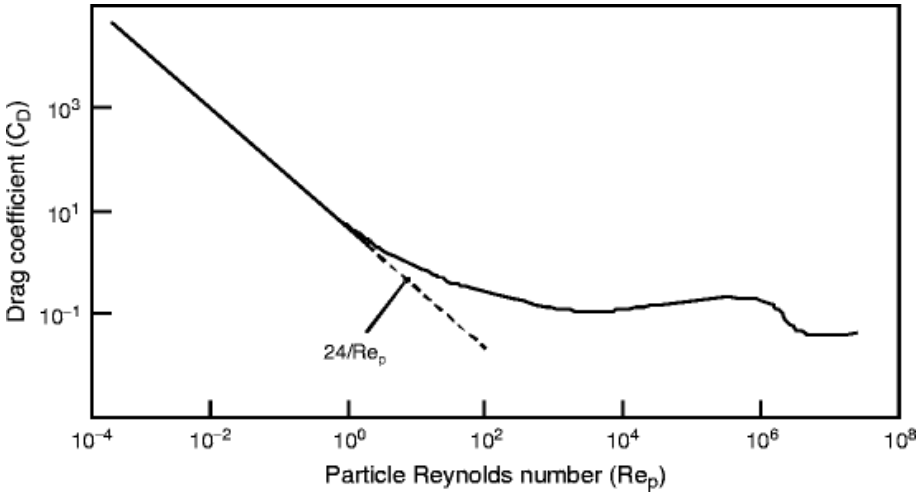

Figure 2. Drag coefficient (C_D) versus particle Reynolds number (Re_p) for spherical particles. (Ortega-Rivas, 2012)

For laminar flow conditions, C_D can be determined from Navier-Stokes equation theoretically as following:

$$F_D = 3\pi\mu u d \tag{3}$$

This approximation offers the best results for the cases when *Re* number approaches zero ($Re_p \rightarrow 0$). The Stokes region can be used with upper limit of $Re_p = 0.2$ with a 2% error in the terminal settling velocity. With the combination of equations 1, 2, and 3 another form of Stokes's law is obtained for laminar flow which is as follows:

$$C_D = \frac{24}{Re_p}\left(Re_p < 0.2\right) \tag{4}$$

C_D becomes independent of the Reynolds number and equal to 0.44 when the flow is fully turbulent (the Newton region).

$$C_D = 0.44\ (Re_p > 1000) \tag{5}$$

Although most of the industrial classifications are carried out in the transitional regime, there are no closed form equations developed to cover transitional area. Instead, C_D is determined by a graph or by some empirical relations.

While separation of fine particles is the most difficult, their separation is a matter of great importance in solid-liquid separation industry. Due to small diameter and low settling velocity of fine particles, Reynolds number is low (Re<0.2). Hence, only Stokes region is

considered to be reasonable in this case by assuming the particles as spherical. Terminal settling velocity can be calculated by Eq. 6. (Will's & Napier-Munn, 2006)

$$u_t = \frac{x^2(\rho_s - \rho)g}{18\mu} \tag{6}$$

where u_t terminal velocity under gravity

As can be seen from Eq. 6, the only adjustable parameter to increase fluid-particle relative velocity is gravitational force since it is not easy to modify particle sizes, densities, and viscosities. It can be achieved by subjecting the suspension to a centrifugal force instead of gravitational field which is described as below by including centrifugal term into Eq. 6:

$$v_r = \frac{x^2(\rho_s - \rho)R\omega^2}{18\mu} \tag{7}$$

where v_r radial settling velocity

R radius of rotation

ω angular velocity

In dynamic type of separators, such as hydrocyclones, the dimensionless expression of Eq. 7 is considered as Stokes number which is obtained from fluid dynamics theory as

$$Stk_{50} = \frac{x_{50}^2(\rho_s - \rho)v}{18\mu D_c} \tag{8}$$

where x_{50} cut size

v superficial characteristic velocity

D_c characteristic diameter of the unit

Separation performance of dynamic separators can be characterized by Stokes number and it is also very important parameter in scaling-up of cyclones. (Svarovsky, 2000)

Classification is widely used in mineral processing which is applied to recirculate oversize materials in grinding circuits in order to avoid further overgrinding of value minerals. In case of their having higher specific gravities than the engaged gangue minerals, they are sent for recirculation for further grinding. The closer a classifier works to an ideal classifier, the more efficient it is. Classification efficiency is a measure of the excellence level of the certain operation and it can be represented with many different ways including mass efficiency, cut size, sharpness of separation and distribution efficiency. (Cohen, 2012)

1.1 Mass efficiency

The mass balance of the particle flow plays a fundamental role in any analysis of a classification process. The flow of particles consists of three parts; the feed, the fine stream and the coarse stream and each stream is described by its own particle size distribution and mass flow (ṁ).

Mass balance of the whole process is:

$$\dot{\mathrm{m}} = \dot{\mathrm{m}}_c + \dot{\mathrm{m}}_f \tag{9}$$

And partial mass balance is:

$$\dot{\mathrm{m}}_0 q_{0i} = \dot{\mathrm{m}}_c q_{ci} + \dot{\mathrm{m}}_f q_{fi} \tag{10}$$

where $\dot{m}_0$ is mass flow of feed, q_{0i} is particle size frequency of the feed, and $\dot{m}_c$, q_{ci} and $\dot{m}_f$, q_{fi} are mass flow and particle size frequency of coarse and fine products, respectively. (Johansson, 2014)

The recovery efficiency of coarse material which is defined as classification function can be described as the following equation:

$$\eta_{ci} = \frac{\dot{\mathrm{m}}_c q_{ci}}{\dot{\mathrm{m}}_0 q_{0i}} = \frac{q_{ci}(q_{0i} - q_{fi})}{q_{0i}(q_{ci} - q_{fi})} \tag{11}$$

The calculation of recovery of fines material is similar to the Eq. 11 and by multiplying both efficiencies, overall efficiency of the classification can be found. (Johansson, 2014)

The information received from the recovery efficiency of coarse material makes it easy to predict the quality of coarse product, which is of interest in the aggregate industry. In order to create an efficiency curve, coarse product efficiency versus the particle size is plotted on a logarithmic scale. This curve is called partition curve or Tromp curve. (Weber & Legenhausen, 2014)

1.2 Distribution functions

Particle size distributions can be represented in the form of frequency distribution curve or cumulative distribution curve. Whilst cumulative distribution curve shows the relative quantity (%) of particles smaller than or equal to size x, frequency distribution curve provides with the information of how frequently each particle size is observed based on number of

particles, surface area or volume of the particles. In order to simplify PSD data interpretation, some statistical parameters can be calculated and reported. Such parameters are as follows:

- Mean - ‘Average’ size of population
- Median - Particle size where half of the population is below/above this point
- Mode - peak of frequency distribution which represents particle size range found in the distribution with the highest frequency
- Percentile - Maximum particle size for a given percentage of sample volume, used particularly in volume-weighed distributions.

The most commonly used percentiles in undersize distributions are D10, D50 and D90. D50, the median, is the particle diameter where 50% of the population lies below/above this value. Similarly, D90 presents 90% of the distribution is below this size and D10 presents the size where 10% of the population lies below. There can be several ways to define means which are based on the method of the collection of distribution data and the analysis. According to the results obtained from laser diffraction method, they can be as below;

D [1,0] Number length mean

D [3,2] Surface area moment mean

D [4,3] Volume moment mean

When the result is displayed as volume distribution, D [4,3] or De Brouckere mean diameter is considered the ‘mean’ and it is appropriate for monitoring the coarse particulates in the size distribution, whilst D [3,2] or Sauter mean diameter is the most sensitive to the presence of fine particulates. (Horiba Instruments, 2017)

Recently, curve-fitting techniques have become more feasible to fit an analytical function to the experimental data and process this function mathematically in further calculations, such as evaluating mean sizes. There are several analytical particle size distributions available for describing empirically-determined size distributions. Such empirical functions are very accurate in size distribution of many particle populations and useful in a broad range of applications. The most commons are:

The log-normal distribution: It is a two-parameter function which is one of the most widely used functions among different types. This model is mostly observed to have a good fit in ceramic powder processing. It can be calculated by the following equation:

$$f(x) = \frac{1}{xln\sigma_g\sqrt{2\pi}} exp\left[-\frac{(lnx-lnx_g)^2}{2ln^2\sigma_g}\right] \quad (12)$$

where *f(x)* is the size distribution function, x_g is the geometric mean of distribution, and σ_g geometric standard deviation of lnx. (Ortega-Rivas, 2012)

It is easy to convert size distribution from one type into another with the log-normal distribution. When all four particle size distributions (by number, length, surface and volume) are plotted on log-probability paper, it can be observed mathematically that they are parallel lines with equal linear spacing. (Saravacos & Kostaropoulos, 2016)

The Rosin-Rammler model is another well-known distribution function which was originally used to represent the results of sieve analysis of crushed coal. It is also a two-parameter function which is usually represented as cumulative percentage oversize. This model is especially suitable for the representation of particles generated from grinding, milling and crushing processes. (Svarovsky, 2000)

$$F(x) = 1 - exp\left[\left(-\frac{X}{X_R}\right)^{n_R}\right] \quad (13)$$

where X_R is a position parameter, n_R is the dimensionless uniformity index, X is the particle size and *F(x)* is the distribution function. (Golmaei, et al., 2018)

1.3 Cut size

In order to the characteristics of classification, Tromp curve is used as the most common approach. This curve can be used with different names; such as grade efficiency curve (Svarovsky, 2000), partition curve (Will's & Napier-Munn, 2006), performance curve (Ortega-Rivas, 2012) and classification efficiency curve (Schmidt & Werther, 2006). Tromp curve mathematically represents the probability of feed fraction with a certain property entering one of the product streams. This curve can also be defined in different ways: (Otwinowski, 2013)

- It determines the amount of classified material that will be collected in coarse product with known size.
- It represents the probability of a particle to exist in the coarse fraction relative to its particle size.

Tromp curve is normally an ‘S’ shaped curve in which the slope of the central portion of the graph indicates the sharpness of the cut; so when the slope is larger (close to the vertical), the classifier is being more efficient. However, depending on the classifier types, partition curves may not always follow the traditional ‘S’ shaped pattern due to the probable occurrence of so-called fishhook effect. For instance, in the wet classifiers, correction might be accounted for the fine particles that exit the underflow with the liquid phase, unlike in air classifiers where gas phase is the medium. The researchers are sceptical about fishhook effect. Some of them assume that it has no physical basis and they argue that the errors originate from the measurements or cause by agglomeration phenomenon. On the other hand, other researchers consider that the effect might be caused by the phenomenon of increased removal of fine particles through the underflow which reduces the separation sharpness. Moreover, it was observed that different particle densities can also cause fishhook effect. (Bourgeois & Majumder, 2013)

Corrected grade efficiency curve (y’) can be derived from the uncorrected curve (y) by Eq. 14. (Tarleton, 2015)

$$y' = \frac{y-R}{1-R} \tag{14}$$

Where *y* is the actual mass fraction of a defined size in the underflow, *y’* is the corrected mass fraction, and *R* is the liquid fraction of the feed recovered in the underflow.

One of the indices taken from T-curve is the efficiency or so-called imperfection index (I) which can be expressed with Eq. 15 where the points at 75% and 25% of the feed particles reported to the underflow are used along with the cut size d_{50}. (Tarleton, 2015)

$$I = \frac{d_{75}-d_{25}}{2d_{50}} \tag{15}$$

Other important parameters are cut size, sharpness index (slope related), imperfection index which is related to the shape of partition curve and probable error, which shows the accuracy of the classification which can be estimated from T-curve. (Otwinowski, 2013)

The most important Tromp parameter is the cut size whose reliable determination directly affects to the predicted result of PSD in fine product classification. Cut size particles are the ones which have equal probability (50%) to end up in the fine or coarse stream. The cut size can be determined from T-curve as shown in Fig. 3, where the ordinate value is equal to 0.5. If it was possible to reach an ideal classification, particles below or equal to the defined size *x*, so-called cut size, would be attained in the fine fraction, while all particle

above that size would be collected in the coarse fraction. However, in real cases, particles in a certain range ($x_{min\,2} \leq x \leq x_{max\,1}$) exist in both fractions which decreases the classification efficiency. (Weber & Legenhausen, 2014)

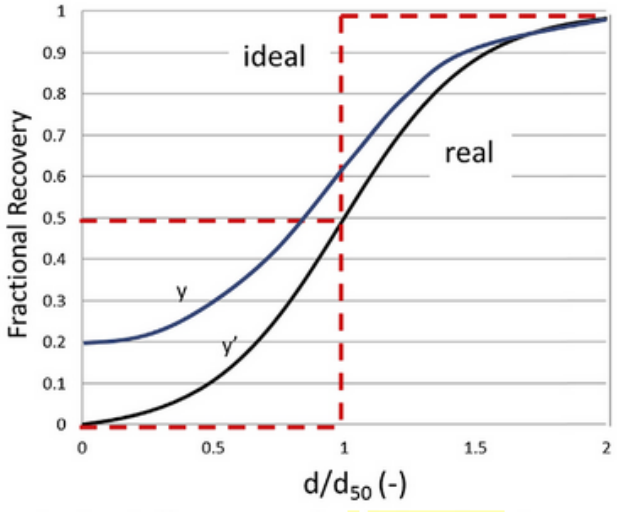

Figure 3. Typical reduced efficiency curve for a hydrocyclone

1.4 Sharpness Index

Another representative value of classification performance is the sharpness index which is defined as the deviation from ideal classification. The slope of the central part of performance curve indicates the sharpness of the separation. The closer the slope is to vertical, the better will be the efficiency. The sharpness of the cut can be measured by the tangent of the separation efficiency curve at d_{50}. However, a simpler way to calculate it is instead of taking a derivate at cut size, by calculating the probable error, so-called Ecart Terra index: (Heiskanen, 1987)

$$E_t = \frac{d_{75c} - d_{25c}}{2} \tag{16}$$

Ecart Terra index is zero for an ideal separation.

The accuracy of separation is determined by the sharpness index which can be expressed as follows:

$$\kappa = \frac{D_{p25}}{D_{p75}} \tag{17}$$

Where κ is the sharpness index, D_{p25} is the size of particles whose probability of entering coarse stream is 25% and D_{p75} is the size of particles having 75% chance of reporting to that stream. Sharpness index (κ) with a value of unity would represent ideal classification. Depending on the feed properties and operating conditions of the classifier, probability values change. Lower sharpness index indicates worse classification. (Ortega-Rivas, 2012)

$0.3 < \kappa < 0.6$ sufficient

$0.6 < \kappa < 0.8$ good

$0.8 < \kappa < 0.9$ very good

Separation sharpness of industrial classifiers operating properly varies between 0.5 and 0.8. (Tomas, 2012)

2 Types of classifiers

Based on the suspension medium, there are two types of classifier which can be categorized as “wet classifier” and “dry classifier”. Wet classifiers are utilized when liquid is used as the medium of suspension and in dry classifiers, separation is achieved by using gas as the suspension medium.

2.1 Dry classifiers

Dry classification method is highly preferred in industries since there is no need to dry and treat the product as in the case of wet classification. It has gained recent industrial interest to control the cut size precisely for fine particles by shifting the cut size to the submicron range in conventional classifiers. It has been proved with experiments that shifting the cut size to the submicron range can be achieved in free-vortex-type classifiers by applying flow control methods. Dry classification usually takes place in air classifiers whose mechanism is based on the respective aerodynamic characteristics of particles. Air classification can handle a broad range of materials, particularly from 2 mm down to 5 µm. (Masuda, et al., 2006)

Air classifier: Air is used as a working medium to classify the product by size and shape in this technology. It is a method of separating powdery, granular, or fibrous materials with respect to their settling velocity, combined with the effect of particle size, particle density, and particle shape. Perhaps the most commonly used air classifier is gas cyclone due to its several advantageous properties. In fact, it has no moving parts, it is inexpensive, easy to maintain, durable to process at high temperatures and it produces a dry product by consuming only a small amount of energy. The primary disadvantage of gas cyclones is that they do not have high collection efficiency for fine particles below 15 μm which is their primary disadvantage (Shapiro & Galperin, 2005). Nowadays, well-designed high efficiency cyclones are available that are effective to collect particles in 2.2 microns aerodynamic diameter. (Gawali & Bhambere, 2015)

A gas cyclone consists of a vortex finder, vertical cylinder with a conical bottom, a tangential inlet near to top and outlets at the bottom and top (Fig.4).

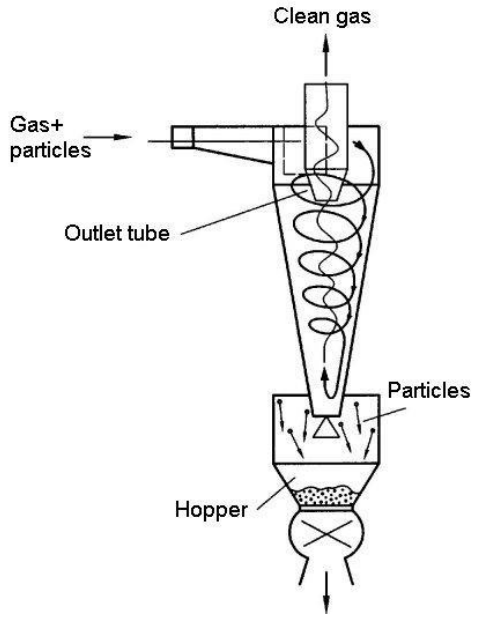

Figure 4. A gas cyclone separator (Anon (b), 2012)

When the feed is blown tangentially into the chamber, the particles are pushed to the outer edges of the cyclone body by centrifugal force developed due to the vortex. Balance between centrifugal and drag force controls the separation. Since the lighter components in the gas suspension have less inertia, they are more easily influenced by the vortex and travel upwards to the top outlet exit while coarse particles flow downward due to the gravity as a thin layer along it as helical path. Separated coarse particles are collected in the hopper which is placed at the bottom of the cyclone. (Johansson, 2014)

Air classification is considered to be effective in separating fine particles down to 5 μm. The separation performance is generally based on the settling rate of particles in gas which is determined by the particle size along with its specific gravity and shape. Settling process is primarily governed by Stokes's law. Depending on the diameter of the unit, cyclones can generate centrifugal forces from 5 to 2,500 times the gravity force. After particles pass into the cyclone body, they quickly reach their terminal velocities depending on their sizes and radial position in the unit (Ortega-Rivas, 2012). Separation efficiency of air classifiers is most commonly analyzed by using a performance curve (Tromp curve) and "cut size" is very important factor in this determination. (Cho & Kim, 1999)

Gas cyclones can be operated at pressures up to 100 bar and temperatures up to around 1200 °C. Diameter of a cyclone can range between 0.05 to 10 m, the concentration of feed changes from 0.1 to 50 kg/m^3 and gas inlet velocity may be in the range of 15-35 m/s. (Ortega-Rivas, 2012)

In order to increase classification efficiency with respect to a single unit, cyclones are often placed in series. Since efficiency increases at the expense of pressure drop, extra attention needs to be given whether it will be cost-effective to achieve high efficiency or not. In some applications, large cyclones are replaced with many small cyclones in parallel, however, it does not always improve efficiency due to unequal gas distribution to each cyclone. Cyclones, as air classifiers, are widely used in food processing in different applications such as in fractionation of wheat flour to separate the coarse particles or fractionation of low protein from high. Another application is particle classification in closed-circuit grinding operations. (Barbosa-Canovas, et al., 2005)

2.2 Wet classifiers

Wet classification refers to separation process of particles into fractions in liquid medium according to particle size or density. The difference in settling velocity between fine and coarse particles is the basic principle for achieving the separation. If the particle density is the same, fines have lower settling velocity than the coarse particles and the settling velocity of light particles is lower than the heavy ones. The working principle of wet classification is no different than the principle of dry classification. However, separation of particles from the liquid requires a drying or dewatering step after the classification. Its advantage over dry classifier is that particle dispersion control is easier. (Ortega-Rivas, 2012)

Hydrocyclone: Separation of particles or droplets from a liquid stream can be carried out by a hydrocyclone device which utilizes centrifugal force and flow pattern generated by fluid pressure. In order to achieve rapid classification, density of particles or droplets must be sufficiently different from the density of the fluid medium. Hydrocyclone was invented in 1891 (Andersson, 2010) and since the 1940s it has been widely used in many industries thanks to its various advantages, such as compact structure, simple design, low operation and maintenance costs, high throughput, and small volume. The main parts of typical hydrocyclone include its top cylindrical section and lower conical section. Although a hydrocylcone has very simple structure, the flow inside can be very complicated due to high shear fluid flow, the layered distribution of particles and the interaction between multiple phases. (Zhang, et al., 2017)

Separation efficiency and cut size are affected by a few parameters, including feed concentration, feed flow rate, PSD, operating pressure, and hydrocyclone geometry. According to Abdollahzadeh et al. (2015), the separation efficiency increases significantly with increasing inlet velocity and particle sphericity and with decreasing volumetric feed concentration. Although it is of great importance to further investigate particle shape effect on the separation efficiency, it has been observed that plate-like particles such as mica are discharged as overflow regardless of it being relatively coarse. (Kashiwaya, et al., 2012)

Hydrocyclones are widely implemented in mineral processing as classifiers due to their ability of being highly efficient at fine separation sizes. One of their applications is in pre-treatment for solid-liquid separation processes in mineral industry, such as dewatering of suspended particles from water stream. Separation mechanism is based on the difference in density and specific gravity of particles and the liquid medium as well as the particle size distribution, according to the Stokes' law. Hence, hydrocyclone is a classifier in which coarse particles pass to the outer vortex while small particles are entrained in the inner vortex (Wu, et al., 2017). It is also reported in the study of Wu et al. (2017) that centrifugal force was the main parameter to determine the separation efficiency of coarse particles, while diffusion effect was the major factor in the separation of fine particles. Hydrocyclones can be employed to classify the particle sizes in the range from 2 µm to 400 µm and with some specialised applications, it is possible to separate fines in the submicron range or coarses up to 1000 µm. Depending on the unit size, their operating pressures vary between 700 kPa for large units and 1 MPa for smaller ones. (Tarleton, 2015)

Mini-hydrocyclones are of increasing interest due to their ability to separate fine particles. The diameter of mini-hydrocyclones is between 1 and 10 mm. The smaller the diameter,

the greater is the centrifugal force created which results in more efficient separation of fine particles (<10 μm). Since the economic importance of nanotechnology in the range of <1 μm is growing rapidly, it highly requires developing new cost-efficient wet classification techniques, especially for micron range. (Yu, et al., 2017)

2.3 Sieving/Screening

Screening is a classification method for dividing a mixture of solid particles having various sizes into two or more fractions based on size difference. The mixture migrates through the screens with specified apertures. Screening is mainly applied for two reasons: for particle size analysis in laboratory tests and for classification or fractionation of particles mostly in mineral processing industry. Sieving and screening terms are used interchangeably as they are very similar, the only difference is that sieving is a small-scale action which is usually used in laboratory tests while screening is an industrial-scale operation. In order to make the separation take place, screen is oscillated, shaken or vibrated and as a result, particles smaller than the screen openings pass through while the bigger ones are retained on the screen. The screening surface may consist of metal bars, perforated or punched plates, plastic cloth, woven wire or silk. Steel, stainless steel, bronze, nickel and monel (nickel-base alloy) can be used as the metal in screening media. Furthermore, the surface of screen may be flat or cylindrical. Apertures size varies between 0.04 and 460 mm, however, depending on the application, it can be even larger. (Ortega-Rivas, 2012)

Although industrial screening is applied for the size separations of broad range, its efficiency decreases sharply with fineness. Dry screening is preferred for the material size above 50 μm, while wet screening is used for down to 250 μm size. Screening can still be used for size separations below 250 μm down to 40μm with different screen types, but air classification is the most suitable to apply below 250 μm as it is much more efficient and cheaper than screening for fines. (Will's & Napier-Munn, 2006) Based on the material passage through the aperture, it can be termed as undersize material, underflow, fines or minus (-) for the passable materials and for the retained materials, it is called oversize material, overflow, tails or plus (+). Desired product may be obtained from either product stream or reject stream.

2.3.1 Screening fundamentals

The best separation by screening is considered to be carried out in such a way that the smallest particle of oversize stream would be bigger than the largest particle of undersize. With such an ideal separation, cut size (diameter), D_{pc} can be obtained at 50% probability which defines that a particle has equal chance to pass through to the undersize or be rejected in oversize product. An example of feedstock, and ideal and real operation can be seen in Fig. 5 (a), (b) and (c), respectively. In the aforementioned ideal case, the size of smallest particle of overflow has been same with the size of largest one of underflow which can be seen in Fig. 5 (b), however in practice, underflow contains particles larger than the cut size, and vice versa as shown in Fig. 5 (c) with an overlap.

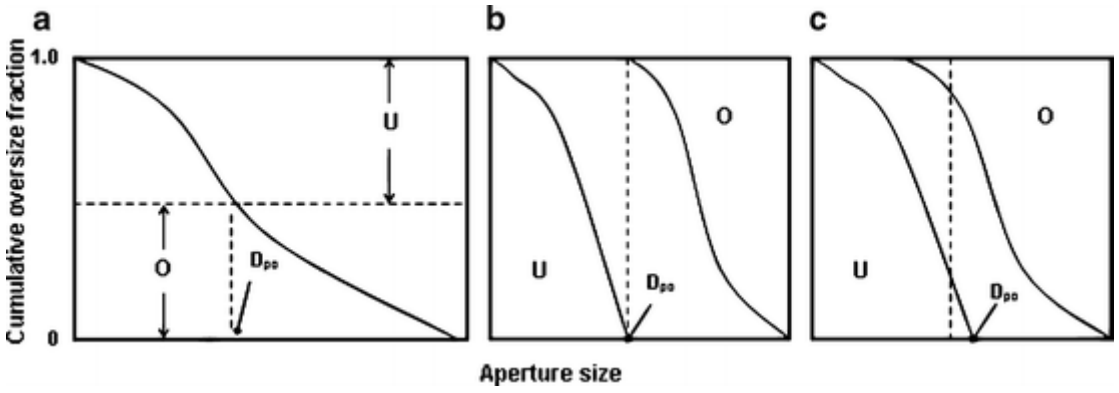

Figure 5. Screening plots: **(a)** feedstock, **(b)** ideal separation, **(c)** real screening (Ortega-Rivas, 2012)

The overlapping is observed to be small when the particles are spherical or close to spherical shape, however it is large when they are needle-like, fibrous, or tend to agglomerate. Clogging of the screen, feed stickiness, and agglomeration are the main problems that are encountered in screening. (Ortega-Rivas, 2012)

Sieves/screens can be classified according to their aperture size or mesh size. Aperture is the minimum free space between the edges of the screen opening and it is used for coarser cloth (w > 12.7 mm), while mesh number is defined as the number of openings (apertures) per linear inch. Although it is an old non-metric US system, it is still widely used for wire cloths w < 12.7 mm (2 mesh). (Tomas, 2012)

The degree of perfection of size separation into the portions above or below mesh size determines the screening efficiency. As there is no single accepted method to define screen performance, it can be represented by efficiency in terms of material recovery at a given

size, or with the mass of mislaid material of each product stream. (Will's & Napier-Munn, 2006)

There are various factors that have an impact on screen conditions and efficiency. These effects include particle size distribution, particle shape, screen angle, tendency to agglomerate, feed rate, feed moisture as well as structural and vibration parameters. Structural parameters can be taken as the width of the screen, wire diameter, mesh size, and screen inclination. In addition, vibration parameters include the amplitude, the vibration angle, and the frequency. (Wang, et al., 2011)

2.3.2 Screen types

Different types of equipment can be used as a unit operation to carry out screening process. Three types are more common among others: grizzlies/belt screens, trommels, and moving screens.

Grizzlies are used to scalp coarse materials (pieces larger than 25 mm) and they are mostly employed in crushing circuits. A grizzly consists of a set of heavy parallel bars where coarse material slides on the inclined bar surface and the material falls through to undersize stream if it is finer than the spacing between the bars (Fig. 6). Vibrating grizzlies are usually used to improve the performance. (Masuda, et al., 2006)

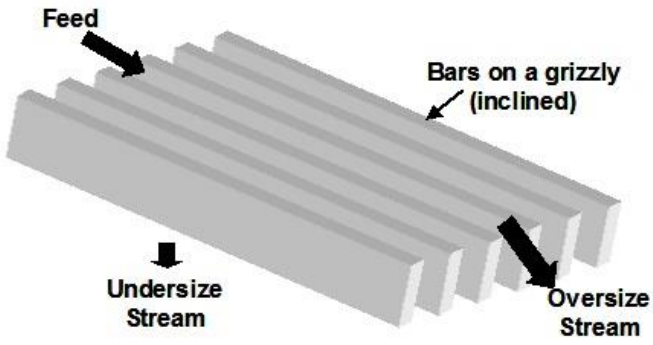

Figure 6. A grizzly (Grewal, 2018)

A *trommel* or *revolving screen* (Fig. 7) is used to separate materials above 1 mm in size. Both dry and wet feed can be handled in a trommel. After the material to be separated is fed at the upper end of the cylinder, the undersize material passes through the screening media and oversize is discharged at the lower end by the help of rotating motion. Although

trommels are cheap, they have disadvantages of being tend to rapid wear and having lower capacities. (Masuda, et al., 2006)

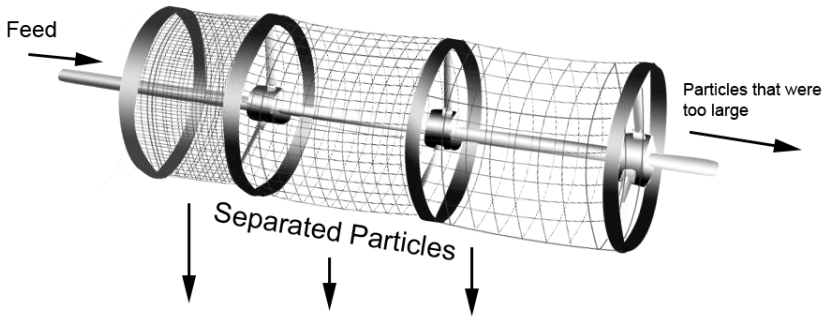

Figure 7**.** Revolving screen used in trommels (Grewal, 2018)

Moving screens are horizontally inclined screens that include reciprocating, vibratory (Fig. 8), sifter, oscillating, and shaking screens. These screens differ from one another according to the motion of surface. In mineral processing applications, the vibratory screen is the most commonly used device. (Ortega-Rivas, 2012)

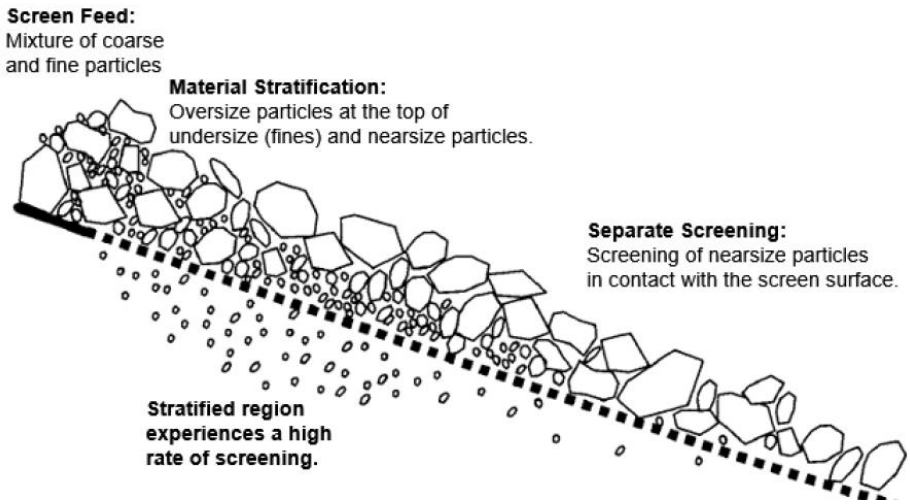

Figure 8. Vibratory screen (Grewal, 2018)

In industrial screens, overall classification efficiency ranges typically from 85 to 95% which might be either separation efficiencies of the undersize or oversize as a product stream. (Saravacos & Kostaropoulos, 2016)

2.4 Magnetic Separation

The classification of magnetic particles based on their magnetic susceptibility is theoretically defined as magnetic separation. This technique has been used in industries for concentrating or removing magnetic materials/particles for many years. When the materials are placed in magnetic field, they are all affected to some extent, although the effect might be too slight for most substances to be detected. According to materials' attraction or repulsion characteristics by a magnet, they can be classified into two groups, such as diamagnetic and paramagnetic materials: (Will's & Napier-Munn, 2006)

- Diamagnetics are repelled under magnetic force to a smaller point of field intensity. Involved forces here are so small that magnetic concentration of diamagnetic materials cannot be achieved.
- Paramagnetics are slightly attracted under magnetic force to a greater point of field intensity and when the external force is removed, the material does not retain the magnetic properties. High-intensity magnetic separators can concentrate paramagnetics.

A special case of paramagnetism is ferromagnetism which involves very high susceptibility to magnetic forces. Therefore, ferromagnetic materials can be concentrated with low-intensity magnetic separators.

Particles are deflected from the main stream if magnetic force is the dominating force over all the other involving forces. The process is schematically represented in Fig. 9.

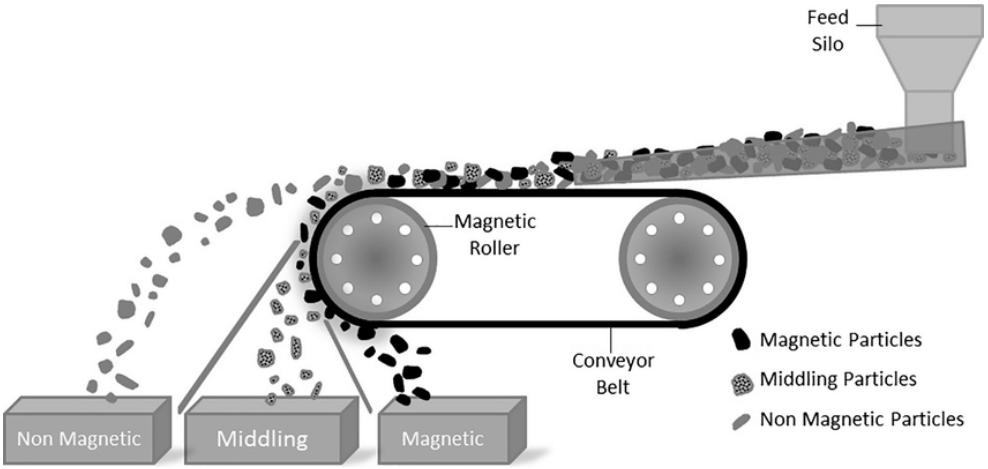

Figure 9. Schematic representation of Magnetic separation process

(Augusto, et al., 2017)

Magnetic separator splits the feed into two or more components. As shown in Fig. 9, material streams are collected as magnetic concentrate, non-magnetic and middling that consists of less magnetic components. After the separation is achieved, each of the product streams is transported out of the device or circulated back for further separation. While the magnetic and competing gravitational, drag, friction or inertial forces tend to separate particles, inter-particle forces reduce the separation efficiency. Selectivity is defined as separation ability of one certain kind of magnetic particles from others, independently of how close their magnetic susceptibilities are (Oberteuffer, 1974). If the particles to be separated are fine particles, the attraction by magnetic and competing forces is very small which results in low separation efficiency and recovery of ultrafine particles (< 5 μm). Thus, some techniques have been developed to increase separation efficiency by increasing effective particle size and shape. Flocculation is one of these techniques where the aim is to form aggregates from ultrafine particles. (Nguyen & Luo, 2016)

In order to separate particles finer than 1 μm, magnetic coating method is the only practically used one in high gradient magnetic separators where the aim is to give magnetic properties to non-magnetics. The principle is based on selective adsorption of the magnetite particles onto a mineral surface in mixed pulp and it renders the coated particles amenable to separate by magnetic separation method. (Prakasha, et al., 1999)

In order to accomplish the separation, drums, belts, and grates are used. In fact, the most commonly used equipment is magnetic drum separator. Throughput rate is dependent upon handled particle size, but depending on the chosen separator type, it can vary from few kilograms per hour up to hundreds of tonnes per hour. (Augusto, et al., 2017)

3 Particle Properties

In the characterization of powdery samples, physical properties of the particles should be taken into consideration to make a mathematical modelling viable. These parameters include the size and shape of the particles, particle density and surface parameters as they affect light scattering during the sizing analysis.

Before discussing the particle properties, it is worth mentioning the fineness categories of particles. According to Merkus (2009), the standardization is as follows:

Fineness (D_{90}):

- Nanoparticles <0.1 µm
- Ultrafine 01-1 µm
- Fine 1-10 µm
- Medium 10-1000 µm
- Coarse 1-10 mm
- Very coarse >10 mm

3.1 Particle size

Particles are the objects in three-dimensional shape that are described with three parameters, such as the length, width and height. Therefore, describing a particle size with a single number is not possible and the irregularity of particle shape makes it ambiguous in particle size analyses. This is the reason why in most sizing techniques, the material is assumed to be spherical, as sphere is the only shape that can be represented by a single parameter (its diameter). In order to simplify the representation of particle size distribution of non-spherical particles, it is convenient to use the concept of equivalent spheres. Below in Fig. 10 is a schematic illustration representing the application of equivalent sphere approach. (Kippax, 2005)

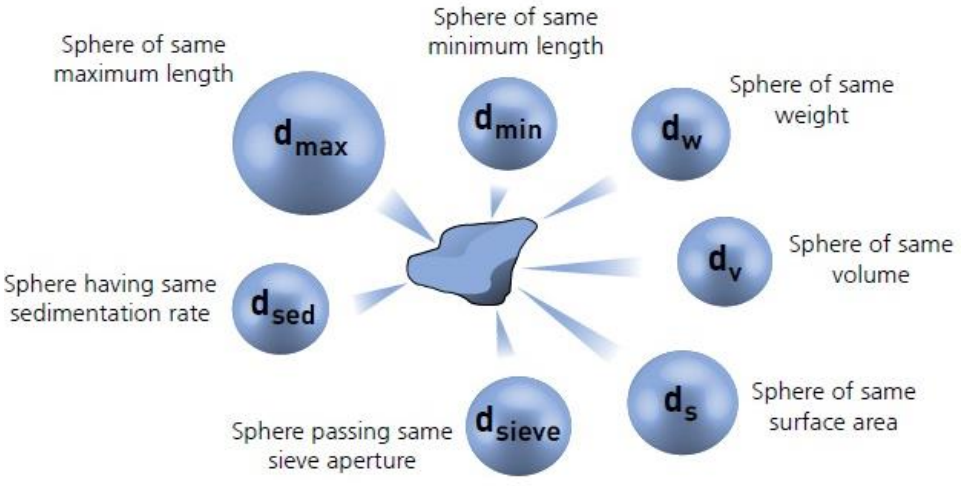

Figure 10. Description of the equivalent sphere diameters (Kippax, 2005)

In Fig. 10, the equivalent sphere models of the same particle are reported by using different sizing procedures. In each case, reported diameter might give a different result for the same

particle as each measurement is based on physical property of the chosen method. Area equivalent diameter is larger in comparison to the other diameters. Diameter reported from sieving is often smaller, since the particle passing the sieve aperture is related to its orientation, showed by its smallest cross section. Stokes' diameter is usually smaller too, it is because the larger surface area of the particles increases the resistance during settling and the orientation of particles with maximum cross section might be perpendicular to the flow direction which also causes increased drag. (Merkus, 2009)

One way of calculating the diameter is to use equivalent circular perimeter diameter D_p as in Eq. 18. In this case it is taken as a basis that the circle has the same perimeter as the particle image silhouette.

$$D_p = \frac{P}{\pi} \tag{18}$$

where *P* perimeter of the particle

The size of some elongated particles, such as rods and needle-like particles is represented by the length (L) or width (W). The length of the particle is calculated from the maximum Feret diameter (F_{max}) which is the maximum distance between two parallel lines on opposite sides of the image of a randomly oriented particle. The width is then estimated from rectangle whose length is $L = F_{max}$ and the area is the same as the image area: (Patchigolla, et al., 2006)

$$W = \frac{A}{L} = \frac{A}{F_{max}} \tag{19}$$

where *W* width of the particle

A area of the particle

3.2 Particle shape

Particle shape is another parameter which has a significant influence on the performance of size measurements of particulate material. Each particle has some shape; different shapes can be expressed with various terms as in Table 1.

Table 1. Various descriptive terms for particle shape (Hogg, et al., 2004)

Spherical	Rod	Dendritic
Cubical	Porous	Spongy
Prismoidal	Acicular	Angular
Platy	Needle-like	Sharp-edged
Flake-like	Fibrous	Sharp-cornered
Granular	Blocky	Rounded

Sphere is the simplest and unique form of a particle, due to its symmetrical property which makes the particle look exactly the same from all directions and its alignment that does not affect the sizing results. Therefore, aforementioned equivalent sphere diameter is used as a representative size for irregular shapes. (Hogg, et al., 2004)

In image analyses, sphericity (*S*) is one of the most preferred ways to express the deviation of a shape from spherical by measuring the ratio between the image area and circle area with diameter D_p.

$$S = \frac{4\pi A}{P^2} = \left(\frac{D_a}{D_p}\right)^2 \tag{20}$$

where
- S sphericity
- A image area
- P perimeter of the particle
- D_a equivalent circular area diameter
- D_p equivalent circular perimeter diameter

The value of sphericity (S) is equal to 1 for the spheres and 0.78 for the squares. (Patchigolla, et al., 2006)

In three-dimensional analysis, a measure of particle shape is defined as the sphericity, ψ, as follows:

$$\psi = \frac{surface\ area\ of\ sphere\ of\ same\ volume\ as\ particle}{surface\ area\ of\ particle} \tag{21}$$

Clearly, $\psi \leq 1$.

If the powder particles are of the same size and geometrical shape of spherical, cubical or rod-like, the size can be represented by the diameter or the length of a side of the particle. (Backhurst, 1991)

3.3 Particle density

Density is a physical property of a material that is expressed as the ratio between the mass of a quantity and the volume of the same quantity. It is an important parameter to be taken into account especially in sedimentation analysis, heat capacity calculations, or calculations of volume or mass of the materials. In particular, particle density is required in mathematical correction of bulk soil samples which contain some amount of gravel and rock fragments. The corrections are necessary to determine fine-soil density, water content or other properties of soil influenced by volume displacement of rocks. (Brittain, 2002)

Particle density refers to the density of collective solid particles. Oppositely, grain density is the density of specific grains. For instance, a bulk soil would have a collective particle density if it contains individual quartz or feldspar, each having its individual grain density. In addition to these, bulk density refers to the density that includes the volume of the pores between particles and pores which already exist inter-individual particles. Grain size and density are both important parameters in such a way that they will be the main parameters in hydrodynamic sorting of particles if the particle shape distribution and complex flow regime are not considered. (Wang, et al., 2015)

3.4 Surface properties

Some particles can be easily charged that then results in the change of force balances within the particulate material and behavioural impact. Electrostatic phenomena have an important role in some industrial applications such as powder coating, xerography as well as sieving where charged particles affect the quality of behaviour of the handled products. In fact, abovementioned effects can include poor flowability, pipe fouling and electrostatic discharge which can be even hazardous when it causes flammable dust clouds and organic vapours to ignite (Yamamoto & Higashino, 2016). The mechanisms of cohesion and adhesion are also related to electrostatic property of particulate material in combination with Van der Waals forces which can play an important role in the behaviour of bulk powder. Whilst cohesion acts between particles as a bond in particle-particle interactions, adhesion

is a mechanism of the particles tendency to stick to a different surface, mostly the surface of processing equipment. (Freeman, 2014)

The porosity of particulate material may also be of importance in particle characterization since the pores might have side effects during size determination. Sedimentation analysis is one of the examples for this phenomenon where the pores need to be filled with liquid and this filling should be integrated with the scattering density since the light scattering at the pore walls can have impact on the scattering intensities of the particles at the angles which then might cause an artefact part in size distribution. (Merkus, 2009)

Pores in the particles can be categorized in three groups based on their sizes.

- Macropores, in which the diameter of pores is larger than 50 nm
- Mesopores, pore diameters range in 2-50 nm
- Micropores, pores diameter is smaller than 2 nm. (Merkus, 2009)

4 Particle Size and Shape Analysis Techniques

In fine particle systems, particulate characteristics of a material determines the system behaviour rather than its bulk properties. Hence, it is crucial to determine the distribution of particle size and shape in product specification and process control. Particle size analysis is conducted offline in laboratories in most of the industrial applications. However, there are some on-line analysis techniques which allow to check and set parameters in real time. (Matsuyama & Yamamoto, 2005)

PSD can have a significant influence on the physical and chemical properties of solids. Hence, this criterion is highly important in science context and quality control. In order to guarantee steady product quality, size distribution must remain constant, as it is shown in the following examples:

- The strength of concrete is highly influenced by the particle size of cement
- The taste of chocolate depends on the cocoa fineness
- The fineness and particle shape of the basic materials of washing powders determines the solubility and flowability.

This list could be extended to a great length. The examples explain the importance of particle size distribution clearly, especially when it assures the quality in the manufacturing of bulk goods. (Tomas, 2012)

4.1 Microscopy and Image Analysis

This technology captures direct images of each particle for generating data and provides users with high-resolution images. By using light microscopy method, subtle differences in particle size and shape can be determined precisely. SEM (Scanning Electron Microscope) and TEM (transmission electron microscope) are two most commonly used imaging techniques which can be preferred according to powder type and its size. The electron is transmitted through the sample in TEM technique, therefore it is necessary to use it for fine-grained (thin) samples. However, SEM can be used for thick samples where electrons are made to scan on the surface of specimen. (Su, 2017)

A scanning electron microscope (SEM) scans the surface of a specimen by using a high-energy beam of electrons and provides information related to its two-dimensional morphology as well as particle size determination. In SEM, significant amount of kinetic energy is carried by accelerated electrons and this energy is dissipated into the sample as multiple signals produced during electron-sample interaction. Obtained signals are transformed into 3D through stereological modelling which helps to understand surface structure of sample. These models mainly focus on the grain shape. In case of spherical particles, their projections are circles on microscopic images. SEM can produce images of sample surface with very high resolution of 10 nm. (Morse & Loxley, 2009)

Transmission Electron Microscope (TEM) is used to observe nanomaterials smaller than 100 nm in size. In TEM, a beam of accurately focused electrons passes through a thin sample and they are scattered according to Bragg's law. TEM equipment can be operated in two basic modes which are diffraction patterns and imaging modes. In order to switch the modes, lens must be adjusted. The advantage of TEM over SEM is its high-resolution ability as TEM uses low wavelength electrons. TEM can view the images at atomic level (which is less than 2 nm). While only morphology of the specimen is obtained via SEM, TEM can provide users with much more information, such as imperfections inside the sample, dislocations, morphology, and its crystallization. (Huseynov, et al., 2016)

Image processing methods contribute to the measurement of particle shape by visualizing the images. One special image analysis equipment is Morphologi G3, manufactured by Malvern Instruments. It is an automated tool with high resolution technique that can characterise particle sizes from around 2 microns up to several millimetres and gives detailed description about morphological properties of particles. Hundreds of thousands of individual particles can be rigorously analysed per one measurement and their size and

shape distribution is constructed automatically from dispersed samples via morphological imaging. It combines particle size parameters, such as diameter, length, width, perimeter, area and sphere equivalent volume with particle shape properties, such as circularity, elongation, solidity and convexity to make comprehensive characterization of both spherical and non-spherical particles possible. In addition to individual particles, the device enables precise detection of agglomerates and other anomalous objects. It is also possible to determine the component-specific chemical identity with the combination of imaging analysis with Raman spectroscopy, in a so-called Morphologically-directed Raman spectroscopy (MDRS) technique (Malvern Panalytical, 2018).

Retsch technology provides high quality dynamic image analysis systems that characterize particle sizes/shapes and these systems are already used in the production and quality control areas of different industries as well as in R&D. These optical systems are CAMSIZER® P4 and CAMSIZER® X2. CAMSIZER® X2 offers more precise and faster analysis for particle shapes and sizes ranging from 0.8 µm to 8 mm. Moreover, CAMSIZER P4 is reliable analyser for wide size range of particles from 20 µm to 30 mm and shapes of spherical and irregularly shaped granulates and bulk materials, pellets and extrudates. (Retsch Technology, 2018)

4.2 Sieving

Sieve analysis is one of the oldest methods used to determine size distribution of particles. The reason behind it being still commonly used technique is its high accuracy, low investment cost, and ease of handling. This method is an alternative to other sizing methods that use light scattering or image processing. By using sieving, relatively broad size range of particles can be analysed quickly and reliably. Depending on the degree of fineness of the sample, appropriate sieving method is selected to be carried out via dry sieve analysis, wet analysis or air-jet sieving.

4.2.1 Dry sieve analysis

In order to determine only the undersize and oversize percentages, single test sieve with a known mesh size is utilized. However, it does not give accurate information about the particle size distribution of the material. Sieve stack is used for this purpose which gives several size fractions and more accurate PSD. Analysis is carried out with a nest or stack

of sieves having known mesh size; each sieve has smaller aperture size in downward direction and each provides the feed for the sieve below. Five or six sieves are usually utilized in one stack and they are clamped onto a mechanical sieve shaker to be vibrated for a fixed time. Such a nest is completed with a bottom pan to collect the fines and a lid at the top to prevent powder loss. (Ujam & Enebe, 2013)

Based on the sample type and its particle size, different types of sieving analyses can be carried out, such as dry sieving, wet sieving and air-jet sieving. In fact, samples might include dry powder, suspension, emulsion, or aerosol. An example of laboratory-scale sieving equipment is given in Fig. 11. Dry sieve analysis is the most often used technique for characterization of dry powders whose particles are coarser than 50 μm. (Merkus, 2009)

Figure 11. Nest of sieves on a shaker (Ujam & Enebe, 2013)

After the vibration time is achieved, residual weight of powder on each sieve is weighed and the percentage weight is determined for each size fraction. In addition to vibration, agitation can be created by using rotation-tapping or ultrasound. (Brittain, 2002)

Sieving rate and sieving end-point can be affected by the following properties of the particulate material: fineness, shape and density of particles, bulk density, moisture content and hygroscopicity-chemical reactivity, magnetic and electrostatic properties, cohesivity of powder, and agglomeration tendency. Dry sieving is suitable for analysing particles from 50μm up to 5 mm. Mass losses during dry sieving are inevitable. However, as long as it is less than 1-2% of the feed material, it is considered to be acceptable. (Merkus, 2009)

4.2.2 Air-jet sieving

When the powder has significant amount of particles smaller than 50 μm, their passage through the equally small apertures is getting difficult in dry sieving as the gravity force of these particles are relatively less than friction force with the aperture walls. In addition, very fine particles adhere to the surface of larger ones. For such samples, air-jet sieving is employed to determine the particle size. Only a single sieve can be fitted in air-jet sieve. Hosokawa Alpine air jet sieve is one of the examples of this machine. In this sieve, particles are agitated by blowing air from a rotating slit through the sieve. Air is then sucked away through the sieve mesh and this assists undersized particles to transport into the air flow which then can be collected in a cyclone or filter. The residue on the sieve is often weighed and starting with a sieve with the smallest aperture is necessary in order to get more points in PSD of a powder. (Merkus, 2009)

4.2.3 Wet sieving

If the above techniques are unavailable or not sufficient, or the cohesion among particles is strong, wet sieving is called for. It is suitable to characterize the particles in size range between 50 μm and 20 mm. Moreover, when the particles are strongly agglomerated or electrically charged, or the starting material is a suspension, wet sieving is preferred. By this method, de-agglomeration can be enhanced, static charges are negated and particles passage through the sieve can be aided. Sieve stack is the same as it is in dry sieving with the additions of clamping cover with nozzle and a collector with outlet (Fig. 12). Spray nozzle is placed above the uppermost sieve by which water is transformed to the sieves and it leaves the sieve stack through the outlet together with the smallest fraction in the collector. Rinsing is finished when the liquid that leaves the sieve stack outlet is not turbid with solid particles any longer. The finest fraction can be recovered via a very fine filter and weighed after drying in case of any requirement for analysis. (Anon (a), 2005)

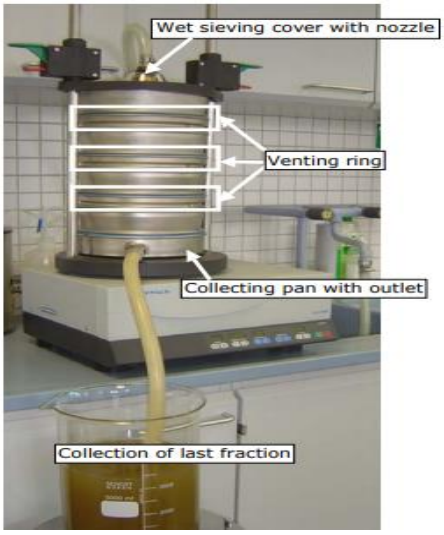

Figure 12. Representation of wet sieving (Anon (a), 2005)

Water is the most commonly used liquid in wet sieving. Alternatively, other liquids with low surface tension can be used. When the dispersant is water, it is sometimes a case that surface tension doesn't allow the suspension to pass through the sieve. In this case, ultrasonic probe is used to initiate the flow (Allen, 2003). After washing the fines through the sieve, sieve fractions are oven-dried and re-weighed. After weighing, electrical sensing zone method is sometimes applied to determine particle sizes. Total time required to perform wet sieving is about 1-2 hours. (Merkus, 2009)

Wet sieving is typically applied for river sediments, clay suspensions, micro granulations, and agricultural soil with high clay content. (Anon (a), 2005)

4.3 Sedimentation

Average Stoke's diameter can be characterised by sedimentation of particles in a fluid. This method is based on the Stokes' law equation which is only valid for spherical particles. In order to determine PSD, the time required for the particles to settle a known distance in a fluid of known density and viscosity is measured. This allows to calculate terminal settling velocity of particles in a fluid which is uniquely related to its diameter. The relationship is described as below:

$$D_{st} = \sqrt{\frac{18\mu V}{g(\rho_s - \rho_l)}} \tag{22}$$

Stokes' law is only applicable for gravitational settling as in Equation 22. Sedimentation of particles takes place via either gravitational settling or Brown motion for the particles ranging from 2 to 50 microns in size. Since the rate of sedimentation is too low for small particles by gravitational settling which is not practical in terms of analysis time, it is normally applied for larger particles. Especially, very fine particles (<0.1 micron) never settle by gravity unless they should be really dense to settle (Hassellöv, et al., 2001). When a centrifuge is used with high gravitational force, it makes the rate of sedimentation higher than Brownian diffusion, even for very small particles. In that case, modification must be done in Stokes' law to take into consideration the variation in gravitational force with distance from rotation center. (Cepuritis, et al., 2017)

Finer particle sizes of sand are usually determined by sedimentation methods, such as hydrometer and pipette. In order to determine the PSD of soils, a combination of sieving and hydrometer is adapted as an international standard. Such sedimentation methods are time consuming, especially, when the particles to be determined are less than 2 μm in size, since relatively large samples are required (10-20 g for pipette and 50 g sample for hydrometer). In addition, they do not give reliable results for particles smaller than 2 μm due to the effect of Brownian motion on the sedimentation rate. (Di Stefano, et al., 2010)

Micromeritics SediGraph has been used for over three decades in particle size determination. Its working principle is based on the highly accurate and reproducible sedimentation methods. Particle mass is measured by X-ray absorption. By measuring particles falling rate under gravity in a fluid based on Stokes' law, SediGraph determines corresponding spherical diameter within the range 300-0.1 μm. The analysis with new generation SediGraph III Plus requires only 2 g of sample and it delivers highly precise particle size information within minutes. Although SediGraph has fully automatic operation and real-time display which allows the users to monitor cumulative mass plot and make immediate changes in procedures if required, it is not able to produce accurate PSD. Also, analysis in the device is temperature-controlled in such a way that liquid properties remain constant during the analysis. (Micrometrics, 2000)

4.4 Electrical sensing zone method

Electrozone technique (or Coulter Counter) is used in various fields to measure the number concentration and particle or droplet size distribution suspended in electrolyte. Electrolyte and particles are forced to travel through the aperture (sensing zone) with two electrodes

on the sides. A particle passing through the aperture will cause a change in impedance between the electrodes as it displaces an equivalent volume of electrolyte and generates pulses. The amplitudes of such conductivity pulses are proportional to the volumes of particles. After the pulses are counted and their heights are measured, the size distribution of particle volumes is determined. It is difficult to measure an emulsion of comparative nature via this method and it is almost impossible to analyse dry powders. In order to perform these, expensive calibration standards are required. (Boschetto & Giordano, 2012)

Errors in measurements are usually originated from coincidence. The instrument supposes that particles pass through the orifice (aperture) singly, therefore each pulse is counted for a corresponding single particle and the magnitude of the pulse is accounted for a single size of particle. Although two or more particles can be interpreted as a single particle by the device in case of close proximity in passing through the orifice or their collision and appearing to be larger than limit. This is called primary coincidence and it results in reduction of observed number of particles. Another case is vertical interaction which is caused by particles passing through the orifice simultaneously. In this case, the magnitude of single pulse will equal the sum of magnitudes, the individual particles would have caused. Under these circumstances, the device relies on the assumption of a single particle having the same volume with the sum of the particles volume. However, observed total particulate volume is not affected, it causes an increase in observed mean size which makes the observed particle size distribution to be flattened slightly and askew towards larger sizes. (Wynn & Hounslow, 1997)

The electrical sensing zone technique is typically an off-line application and it is used as a particle counter for narrow PSD, typically covering the range from 0.5 to 1000 μm. In-line measurement can only be applied for product streams if they have a low particle concentration in a conductive liquid. By this method, solutions of particles at low concentration are mostly analysed. The reason behind low particle concentration is to ensure that particles pass through the orifice one by one. The analyses are performed with a high-resolution Coulter Multisizer II or Multisizer III device. The measurement time is approximately 1-5 min. The obtained result consists of the graph which shows the cumulative and differential particle volume or number distribution and information related to particle statistics, such as mode, mean and median particle diameter. (Merkus, 2009)

4.5 Laser diffraction method

Laser diffraction or laser light scattering technique has become one of the most popular methods in particle size analysis due to its reliability, speed, easiness to use, and reproducibility. Laser diffraction is used to analyse the size of from 0.02 µm up to 3.5 mm. The sample can be wet or dry, depending on the dispersion media. In dry sample, dispersion media is air and in wet samples, it is a suitable liquid in which particles are insoluble. It relies on the fact that when incident light falls on a particle through a dispersion media, the light is scattered at an angle depending on the particle size. If the size of particles decreases, the scattering angle is observed to increase logarithmically, and the angle is getting narrower if the particles are large. (Kippax, 2005) This scattering is not only dependent on particle size, but also on wavelength and polarisation of the light and the refractive index of particle and its surrounding medium (Bowen, 2002).

The measurement and correlation of PSD to laser diffraction pattern rely on an appropriate optical model. These models include the Fraunhofer approximation and Mie theory. Volume equivalent sphere diameter is the typical approach to report particle size. Mie theory gives a more precise solution in the measurement of particle size distributions from light scattering data. The use of Mie theory requires to presuppose the refractive index of particles and the medium, and the imaginary part of particles refractive index. Refractive indices for a wide range of materials and media can be easily found from literature or measured but it is difficult to find indices for imaginary parts (Matsuyama & Yamamoto, 2005). Regardless of the particle's being small or large, transparent or opaque, the scattering intensities can be predicted for all types. Primary scattering intensity for particle surface is allowed by Mie theory with the intensity predicted by the difference between particle refractive index and the refractive index of the dispersion medium. Secondary scattering is also predicted by using the light refraction inside the particle. The latter phenomenon is particularly important for particles whose diameter is below 50 microns, according to the international standard for laser diffraction analyses [ISO13320-1 (1999)]. (Kippax, 2005)

The Fraunhofer approximation is a more simplified approach which does not require the user to know the optical properties of the sample. It considers particles being measured to be opaque and light scattering to be at narrow angles. Thus, this approach provides accurate results only for large particles (>50 microns) and does not give a correct assessment for fine particle fractions. This is the reason why extra caution is required in the Fraunhofer optical model while working with the samples having particles below 50 microns or relatively transparent particles. (Matsuyama & Yamamoto, 2005)

Typical scheme of laser system is represented in Fig. 13. It includes laser which is to provide a source of intense light of fixed wavelength, a set of detectors to measure the pattern of the light in various angles, and a sample presentation system. (Kippax, 2005)

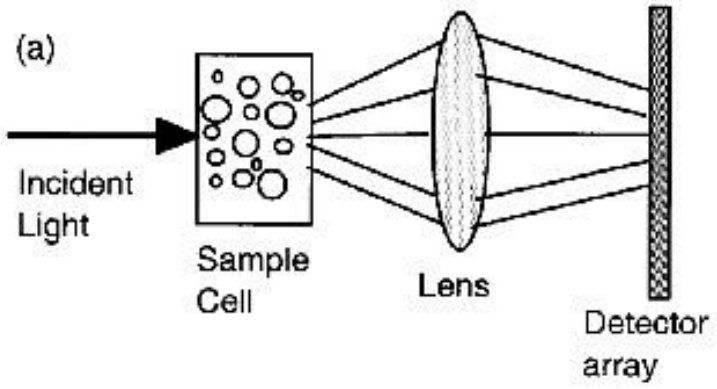

Figure 13. Schematic representation of light diffraction through a suspension with lens and detector (Bowen, 2002)

When the particles pass through a laser beam, they scatter the light and this light is collected with a range of detectors at different angles in the forward direction. As mentioned earlier, diffraction angle is inversely related with the size of particle (Bowen, 2002). According to the results of the sensor (photodiode), particle sizes and distribution are obtained. When inserting the sample to the device, concentration of particles should be low to avoid multiple diffractions of laser light as well as high enough to let particles scatter enough lasers light for detection of the sensor. The optimum obscuration for wet dispersion is in the range of 10-15% (Zárybnická, et al., 2012). In Malvern application notes, it is recommended to use obscuration range dependent on particle size as in the table below.

Table 2. Recommended obscuration ranges for different particle sizes.
(Malvern Instruments Ltd, 2013)

Particle size	**Obscuration range**
Fine particles	~ 5 to 10 % (less than 5 % may be required for <1 µm
Coarse particles	5 to 12 %
Polydisperse samples	15 to 20 %

Malvern Mastersizer 2000 and 3000 are the laser diffraction instruments that are applied worldwide in the analysis of broad range of particles. Mastersizer has automated operation and well-optimized optical design that allows diverse range of particles to be characterized effectively. The device sees the particles as spheres and gives their volumetric particle size distributions (Ferro & Mirabile, 2009). In order to determine the PSD, the Mastersizer apparatus uses two light sources: red light with the wavelength of 633 nm and blue light with the wavelength of 470 nm. In addition, the instrument takes 1000 data snapshots per second with three sequential runs which then is computed by the software as the average of these runs to give a final grain size. (Malvern Instruments Ltd, 2013)

II Experimental part

5 Aim of the work

The aim of this work was to measure particle size distributions of a number of industrial side streams by using laser diffraction and sieving techniques. For this purpose, PSD analysis was initially carried out by using Mastersizer 3000 to obtain an estimation about the size. Then, according to the results, test sieves were selected for each sample and after suitable amplitude range was found for sieving, the experiments were carried out. Afterwards, the feasible operational parameters for LD, such as the selection of stirrer speed, obscuration rate, measuring time and ultrasonication usage were selected by conducting some analyses. PSDs of raw samples were again analysed with Malvern Mastersizer 3000 by using the selected parameters and the results from both methods were compared. In addition, fractionated sub-samples were analysed by LD method to observe the median shifts.

6 Materials and methods

Measurement of particle size distributions was carried out for 19 samples in total including bottom ash and fly ash samples from different processes, green liquor dregs, tailings, $CaCO_3$, coating sludge, deinking flotation reject foam, lime and construction waste (See Appendix 1). For sieving experiments, electromagnetically driven 3D test sieve shaker of Haver & Boecker was used (Haver Eml Digital Plus). Cleaned sieves were dried in Memmert oven at 65 °C. Volumetric particle size distributions of raw samples and fractions from sieving experiments were analysed by laser diffraction method by Malvern Mastersizer 3000 equipped with Hydro EV as the feed unit.

6.1 Sieving analyses

Sieving process requires some preparatory steps before starting the actual analysis, such as sampling, the selection of test sieves and measuring weight of the empty sieves and the sample. After the sieving is done, data is evaluated, and the sieves are washed and dried.

6.1.1 Sample preparation

The main step in sampling was to take the samples from various locations of the container and mix them together and afterwards measure their weight in order to assure the quality. The amount of material to be sieved was decided so that it was in the range of the handling capacity of top sieve to avoid overloading and enough to obtain representative sub-samples. In most of the experiments, 1000 g of feed sample was used. However, only 350 g was required to sieve the ash sample obtained from bark combustion (#16) as the bulk density of the sample was low. In addition, the preparation of the bottom ash sample resulting from co-incineration (#5), needed manual separation before the sieve analysis as "nail-like" and big irregularly shape particles were present in the sample which might have damaged the sieve medium. Although they have been removed from the feed sample, their mass has been added to the size fraction of the top sieve with the aperture width of 5 mm.

Besides the dry samples, some of the samples had excessively high moisture content to start sieving. Therefore, those samples were weighed and dried overnight in the oven at 105 °C and afterwards cooled in a desiccator until the samples reached room temperature. Particularly, lime/slaked lime ($CaO/Ca(OH)_2$) and fine fraction of tailings from carbonate mine, samples 12 and 17 respectively, formed aggregates after drying and this is why the aggregates were crushed carefully before sieving in order to avoid incorrect results in the calculation of size distributions.

6.1.2 Steps of sieve analysis

Particle size analyses were performed with Haver & Boecker sieve shaker equipment (Fig. 14). Test sieves were available in different opening sizes, from bottom to up, as 25 µm, 36 µm, 50 µm, 75 µm, 100 µm, 150 µm, 200 µm, 300 µm, 500 µm, 800 µm, 1250 µm, 2500 µm, 5000 µm. Test sieve frames were made from stainless steel with the medium of woven wire cloth or robust plates with square meshes in accordance with DIN ISO 3310-1. Sieves were selected based on each sample properties. In order to make this more accurate, initially the PSD of each sample was analyzed by using Malvern Mastersizer 3000 and sieve sizes to be used in the stack were decided according to obtained results from each graph.

Figure 14. Sieve analysis equipment with a set of different sizes of sieves (left), test sieve (up right) and separate control unit (down right).

The next step was to weigh empty sieves, the collecting pan and the test sample. Afterwards, the test sieves were stacked together with increasing aperture size with the pan at the bottom of the sieves for collecting the particles which pass through all the sieves. The sample was placed on the top sieve, closed with the lid and the stack was fastened to the sieve shaker. Amplitude was usually adjusted in 1-1.5 mm range in this study and the time was set to be in 10-30 min range initially. After setting a suitable amplitude and sieving time, sieve shaker was started. Thanks to the three-dimensional sieving motion of the shaker, the sample is shaken through the mesh in vertical direction and distributed over the sieve surface in a circular motion.

The stack of sieves was kept agitating for the initially adjusted period of time; when the shaker stopped, the sieves with their retained fractions were weighed and placed on the shaker again. This process was continued up to a point where no changing in the mass of the sample on respective sieves was observed during back weighing. After sieving process

was finished, the weight of particles retained on each sieve was measured and the passing and retained percentages were calculated.

6.1.3 Cleaning of the sieves

When the sieving was complete, the fractions were recovered from each sieve. In some cases, near-mesh particles were trapped in the sieve mesh and blocked the opening. Those particles were removed from the sieve by turning it upside down and tapping it slightly on a table. Sieves with a mesh size above 500 microns could be cleaned easily with sprayed water. However, sieves with a mesh size below 500 microns needed special care. They were rinsed with water in order to remove the bulk of residues and then submerged into an ultrasonic bath. The high intensity of ultrasound creates bubbles by cavitation action that implode on contact with all surfaces and removes near-mesh particles from fine sieve medium.

Water was used as cleaning agent and each cleaning in the ultrasonic bath took approximately 2-3 minutes. Sieves were thoroughly rinsed with water again after ultrasonic bath. Finally, the sealing ring of each sieve was removed and the sieves were dried overnight in the oven at 65 °C. The drying temperature had been decided so that it should not warp the fine metal wire and reduce the tension of the woven medium inside the sieve frame. After the sieves were dry, the sealing ring was put on each sieve again.

6.2 Malvern Mastersizer 3000

Particle size distributions of raw samples and the fractions obtained from sieving experiments were analyzed with Malvern Mastersizer 3000 which is a compact optical system that uses laser diffraction technique (Fig.15). Fraunhofer light scattering approach will be used in this work as it does not require to know refractive indices of the samples. Some preliminary analyses were carried out in order to find suitable operating conditions, such as stirring rate, measurement time, obscuration level and ultrasonication effect.

When settings were completed, the background was checked to assure the cleanliness of the system and the sample was then dispersed in water in up to a point where the obscuration level was between 5-15 %. Sample aliquot was added to the 1000 mL beaker by pipette or spatula and the suspension recirculated through the Mastersizer’s

measurement cell via the Hydro EV dispersion unit. The operational parameters were selected based on their influence on the results after carrying out abovementioned analyses. Mostly, 15000 snapshots were performed per each measurement (15 seconds) with background measurement time of 30 s as it should be double the measurement time and no ultrasound treatment was applied. After each measurement, the dispersion head was raised out of the beaker, the system was enabled for normal cleaning (3 circles) and new sample was dispersed. Cleaning/calibration process was carried out automatically, so only the filling and emptying of the beaker needed manual work.

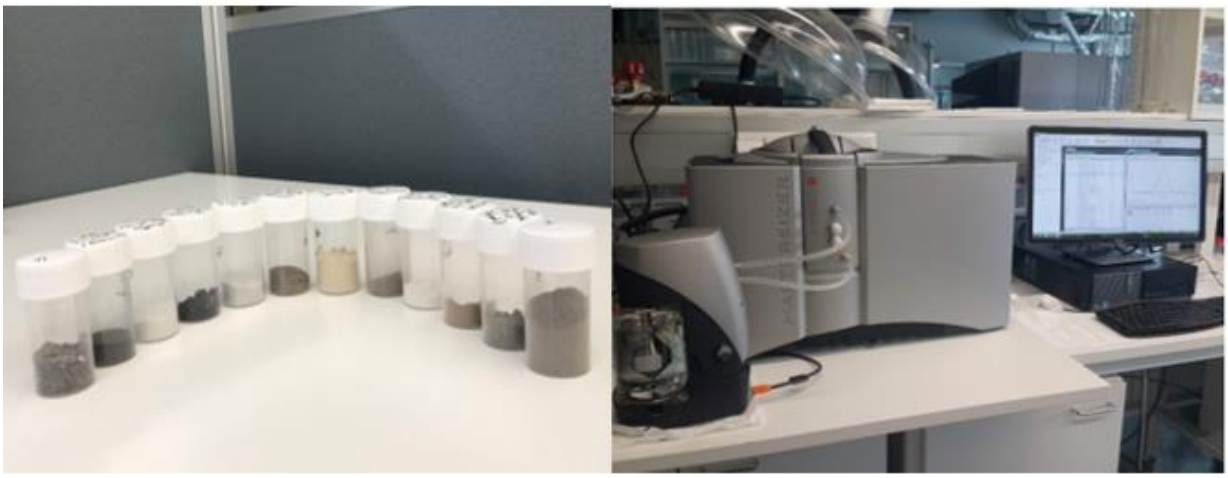

Figure 15. Raw samples (left) and Malvern Mastersizer 3000 particle size analyser equipped with Hydro EV unit (right).

7 Results and discussions

Altogether, volumetric distributions of 19 different samples were analysed by Mastersizer 3000 particle size analyser and 13 out of their ‘sievable’ ones were analysed by sieving technique by which cumulative mass fraction curve was obtained. The results from both analyses were compared. In addition to this, representative sub-samples were taken from each sieve fraction and they were analysed by laser diffraction method again to observe the median shift and distribution width (83 fractions in total). In order to select operational conditions for sieving and laser diffraction methods, some experiments have been carried out on the randomly selected sample #14. Stirring rate of 2500 rpm with no ultrasonication effect with the measurement time of 15 s was selected as the reference in the representation of Mastersizer results below as the average data of 5 measurements.

7.1 Laser diffraction measurements

7.1.1 Selection of measurement duration

Malvern Mastersizer 3000 works as a closed loop system with pump by which the suspension is carried through the measurement cell and circulated around continuously. In order to all the suspended particles be accurately analysed and to provide representative particle size the optimal duration of analyses should be found. The measurement time needs to be long enough so that the particles in dispersion unit can circulate though the measurement cell and they can all be measured consistently during the run. It depends on the size of particle population in a way that if the size distribution of the sample is broader or particles are coarse, then longer measurement times are required.

In order to determine the effect of the measurement duration on PSD, sample #14 which is fly ash from peat and biomass has been randomly chosen to be analysed. The measurement times were selected to be 5 s, 10 s, 15 s and 30 s for the runs of the same sample and the analysis started with a constant delay after dispersing the sample in the beaker. The influence was studied by measuring the Sauter mean diameter D [3,2] of the sample and the main results from the analyses are summarized in Fig. 16.

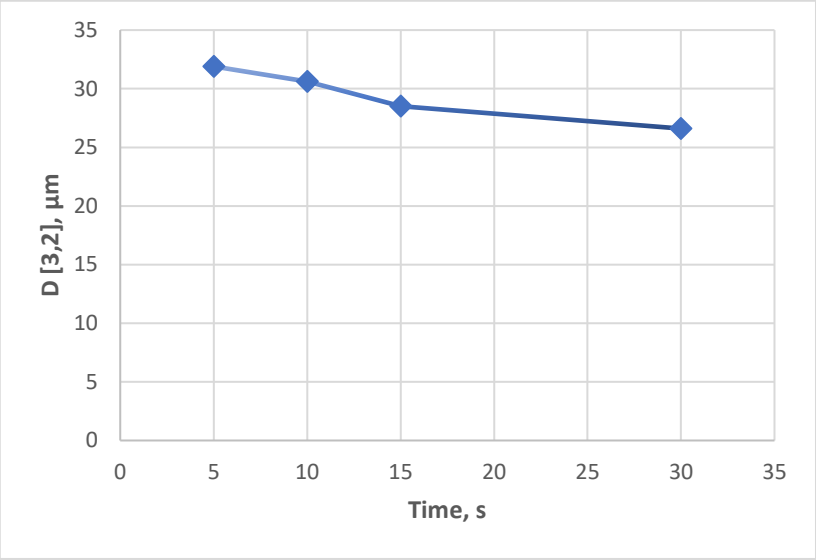

Figure 16. Sauter mean diameter versus measurement time. Runs were performed at stirring speed of 2500 rpm and obscuration varied between 5 and 10%.

Fig. 16 shows the decrease in Sauter mean diameters of sample #14 as the measurement time increases. The instability, 16% size reduction, at the shorter times is presumably due to not having enough time to completely represent the aliquot in the dispersion. The decrease of the surface mean size in 30 seconds might be due to the individual particle fracturing or breakage while operating at longer time in 2500 rpm stirrer speed to representatively circulate all particles through the cell. Size reduction was also observed in each parallel 5 runs while using 30 s measurement time. Due to uncertain effect of long measuring time, 15 seconds of measurement time corresponding to 15000 snapshots was used as the reference time in the PSD determination of the original raw samples.

7.1.2 Selection of stirrer speed

The purpose of the stirrer is to ensure the homogeneity of the dispersion by preventing sedimentation of particles in the measurement unit and to circulate particles of all sizes through the measurement cell. When the particles have densities above the density of the suspending fluid, it is necessary to make sure that stirring speed is high enough to prevent those particles from settling out. In order to choose optimum stirring rate for the further analyses, the effect of stirring speed was experimented on the sample #14 again, as this sample does not have very broad or very narrow size distribution. The rotation speed of the stirrer was varied between 1000 to 3500 rpm with the increments of 500 rpm. The effect was studied on the percentiles of D (10), D (50) and D (90) of the particle size distribution and the main results are summarized in Fig. 17.

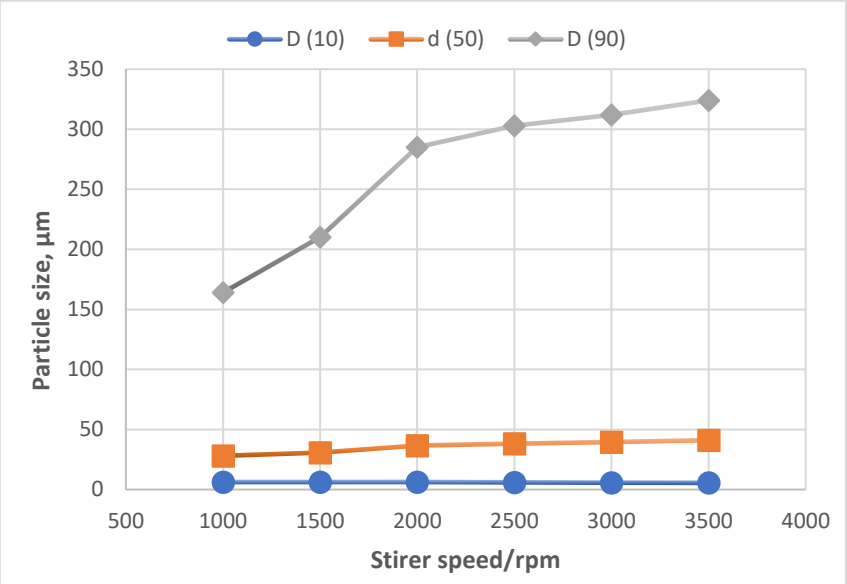

Figure 17. Relationship between three percentiles and the stirrer speed. Runs were completed with 15 s measuring time and the results are given as average of 5 runs.

As can be seen from the graph above, D (10) value seems not to be influenced by the change of stirrer speed while D (50) value increases significantly from 28 µm to 41 µm. The decile, D (90), increases approximately by 43% until the rotation of the stirrer is 2000 rpm and in higher speeds, from 2000 rpm to 3500 rpm, it increases by 12%. Since D (90) represents the limit between the largest 10 % of particles and all others in the suspension, it is wise to select the stirrer speed by studying this value. The reason why particle size is smaller at low stirring speeds might be due to the poor representation of the larger and denser particles as the energy provided by the stirrer is too low to prevent them from sedimenting and to transfer all the sizes from the beaker to the measuring cell. However, particle size is significantly influenced when the stirrer rate changes from 2500 to 3500 and it was also observed that the suspension splashed out from the beaker at very high speeds, which might cause changes in the properties of measured samples. Taking into consideration the obtained results of this analysis, 2500 rpm seems to be suitable for stirrer speed and it will be used as the reference for the further analyses.

7.1.3 Selection of ultrasonication energy

When the aliquot has been added to the beaker, ultrasonic energy can be applied to the suspension where it creates cavitation in the liquid and this might lead to breakage of agglomerated particles due to the energy from expanding air bubbles. However, it is also a

case that ultrasonic treatment may cause re-agglomeration, depending on the analysed sample and liquid. If sonication effect is used for long times, it can cause thermal heating of the suspension that could falsify the results. In order to study the influence of ultrasonic treatment on particle size, the aliquot (sample #14) has been measured in three stages where in the first 5 records, there is no US applied, in the second stage (from record number 5 to 10) 50% of US treatment for 60 seconds has been applied and in the last step (from record number 10 to 15), the particle size after-US has been measured as represented in Fig. 18.

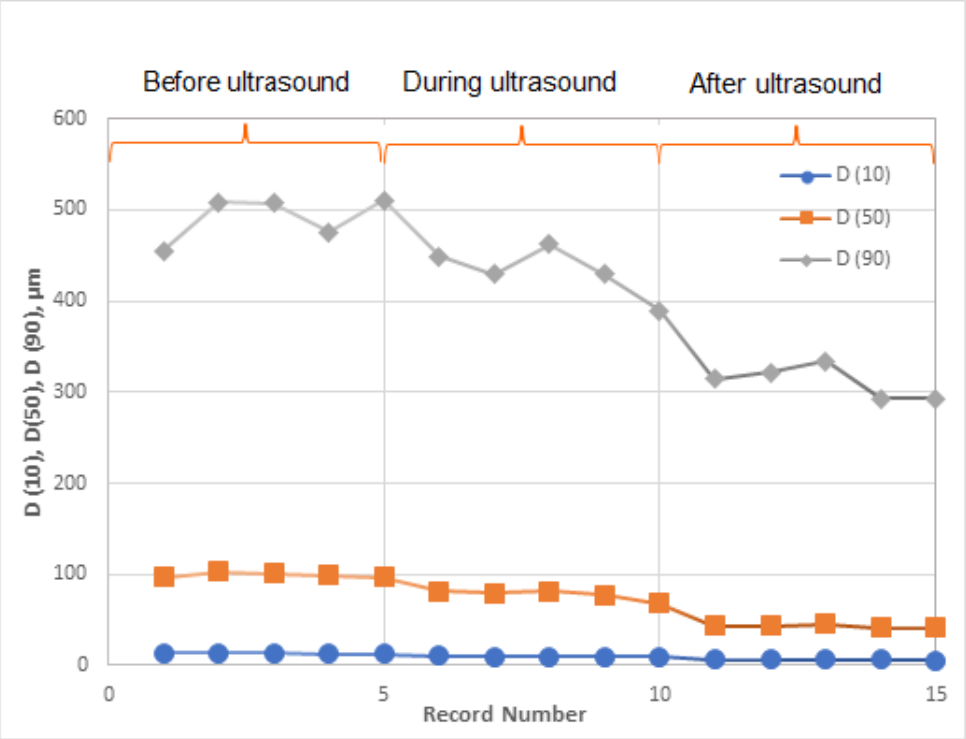

Figure 18. Change in D (10), D (50) and D (90) values for measurements before, during and after ultrasound.

There are slight variations in the D (90) value even before US treatment applied, and it is followed with a rapid decline of the D (90) size during ultrasonication which might be a good condition for the breakdown of agglomerates. When the ultrasound is turned off in the third stage, the particle size seems not to be stable which might be due to the further breakage of primary particles. During the application of US treatment, the existence of air bubbles in the beaker was observed and these bubbles enhanced de-agglomeration process and since the concentration of individual particles increased as a result of de-agglomeration, the obscuration level kept increasing.

The decrease of PSD during US treatment was observed in most of the cases due to the breakage of agglomerates, however, the PSD of some samples even increased during US.

Due to the uncertainties of US influence on the particle size distribution, it was decided not to apply US when the PSD of raw samples were measured. However, if in any cases it is desired to be used, it should be applied for a short time in order to avoid the breakage of primary particles and other changes that may occur as a result of its thermal effect.

7.1.4 Selection of obscuration range

The optical concentration of the sample is known as obscuration level and stability of the obscuration during a measurement is desired. If it is decreasing during a wet dispersion, it indicates that particles are lost from the system which might be presumably due to the dissolution. The obscuration level needs to be high enough depending on the measurement duration so that required number of snapshots is obtained (for instance, 15000 snapshots in 15 seconds). Similarly, it should not be too high because it might cause multiple scattering. The influence of obscuration level on PSD is illustrated in Fig. 19, where the obscuration levels are 3%, 9%, 14% and 19%.

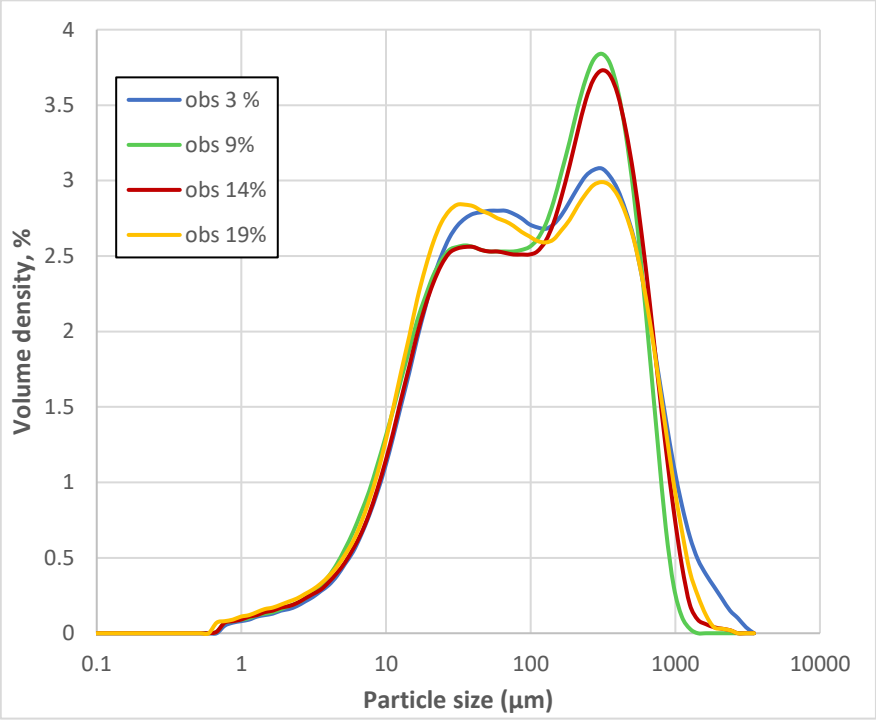

Figure 19. Effect of obscuration level on PSD of sample 14.

When the obscuration level was 3% and 19%, volume density of the same size particles was smaller than the volume density at 9% and 14%. The reason why the size distributions measured at 3% and 19% are similar can be that particle concentration is not enough at 3% and multiple scattering has been observed at 19% which causes the laser light to be

scattered to higher angles and then it leads to underestimation of particle size; as higher angle indicates finer sizes. By combining these results with the literature information as mentioned earlier in Table 2, the obscuration level that will be mostly used in this work is within 5-15% range.

7.1.5 PSD analysis of original samples by Mastersizer 3000

There were 7 ash samples collected from different processes to be analysed. Their results are summarized in one graph that is shown in Fig. 20 where sample number 1 refers to ash (from bark combustion), 4 to fly ash (from co-incineration), 7 to fly ash (from biomass power plant), 11 to ash (from gasification of bark on $CaCO_3$ bed), 14 to fly ash (peat + biomass), 16 to ash (from combustion of bark) and 20 to fly ash (coal).

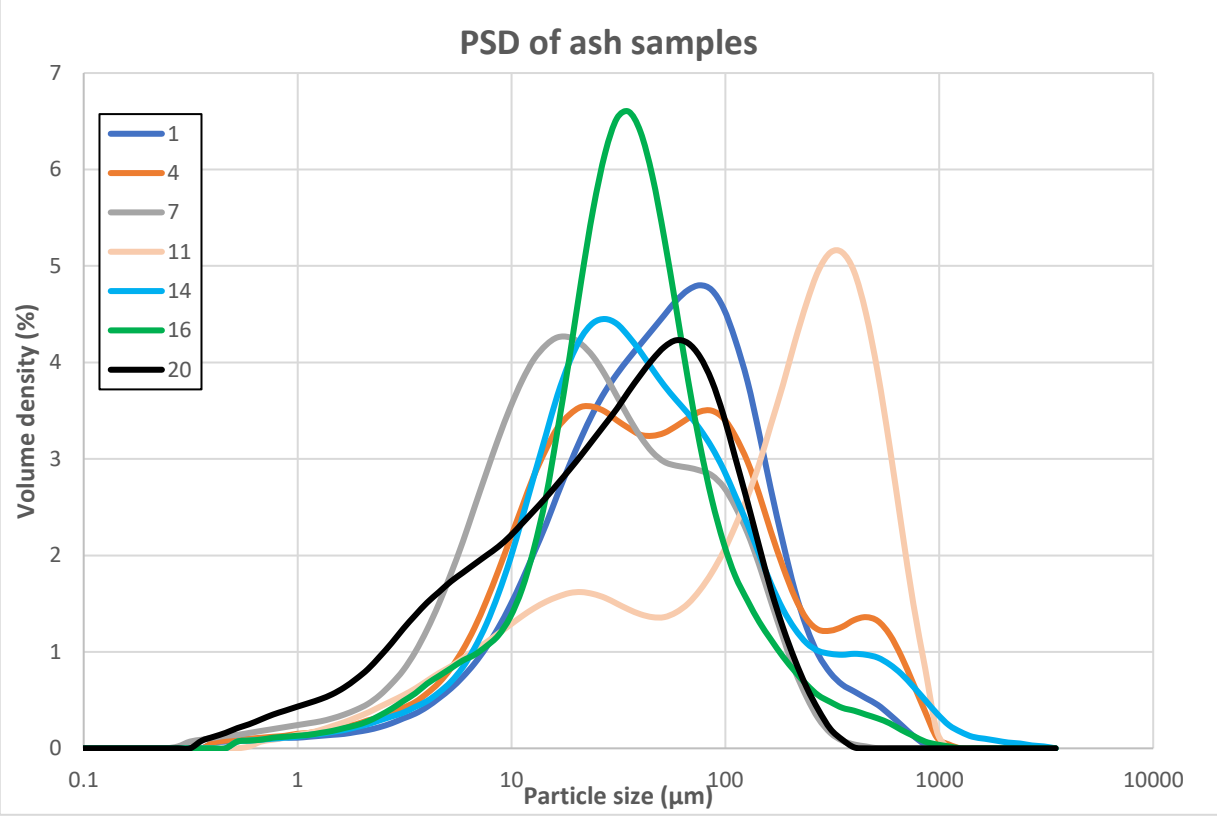

Figure 20. Volumetric particle size distributions of ash samples. Operating procedures: stirrer speed of 2500 rpm, measurement time of 15 s and obscuration between 5-15%.

Beside volumetric distributions of samples, D (10), D (50), D (90) values and volume and surface area means were obtained. The overall results are represented in Table 3.

Table 3. Derived results from particle size measurements of the ash samples

	Particle size, µm				
Sample No.	**D (10)**	**D (50)**	**D (90)**	**D [4;3]**	**D [3;2]**
1	11.4	54.5	184	85.5	20
4	8.9	46.7	304	110	16.8
7	5.4	24	119	45.7	10.2
11	9.2	180	548	231	22.8
14	10.1	40.8	268	112	18.7
16	9.9	36.6	123	61.9	17.6
20	3.8	33.3	126	51.9	8.96

Particle size of samples #7, 16 and 20 are similar as their percentile values and distribution widths are close to each other except the case that sample 20 does not contain particles bigger than 500 µm compared to others and the majority of particles is smaller than 130 µm. Sample 16 has very 'symmetric' frequency distribution curve which indicates that size of particles is uniform where 90 % of the population is finer than approximately 125 µm and it only has 10 % of bigger particles (up to 1 mm). On the other hand, it becomes clear by monitoring D (10), D (50) and D (90) values of sample #4 that these three percentiles of the sample differ significantly from one another and the frequency distribution curves are also non-uniform which indicates that the sample contains very coarse and fine particles and it is difficult to determine the main particle size. Samples #11 and 14 have the similar trend with sample #4. However, D (90) of volumetric particle population of sample #11 is as high as 548 µm which is the largest size among the ash samples. In addition, while 90% of sample #1 contains particles finer than approximately 190 µm, 10% of the rest particle population is changing up to 1 mm.

PSD of carbonate and lime based samples are presented in Fig. 21 where sample #3 refers to $CaCO_3$ (from chemical recovery cycle), 12 to lime/slaked lime ($CaO/Ca(OH)_2$), 13 to lime kiln dust and they are the side streams from kraft pulp mills. In addition, sample 17 is fine fraction of tailings, 18 is coarse fraction of tailings and sample 19 is thickening pilot underflow and those are collected from carbonate mine.

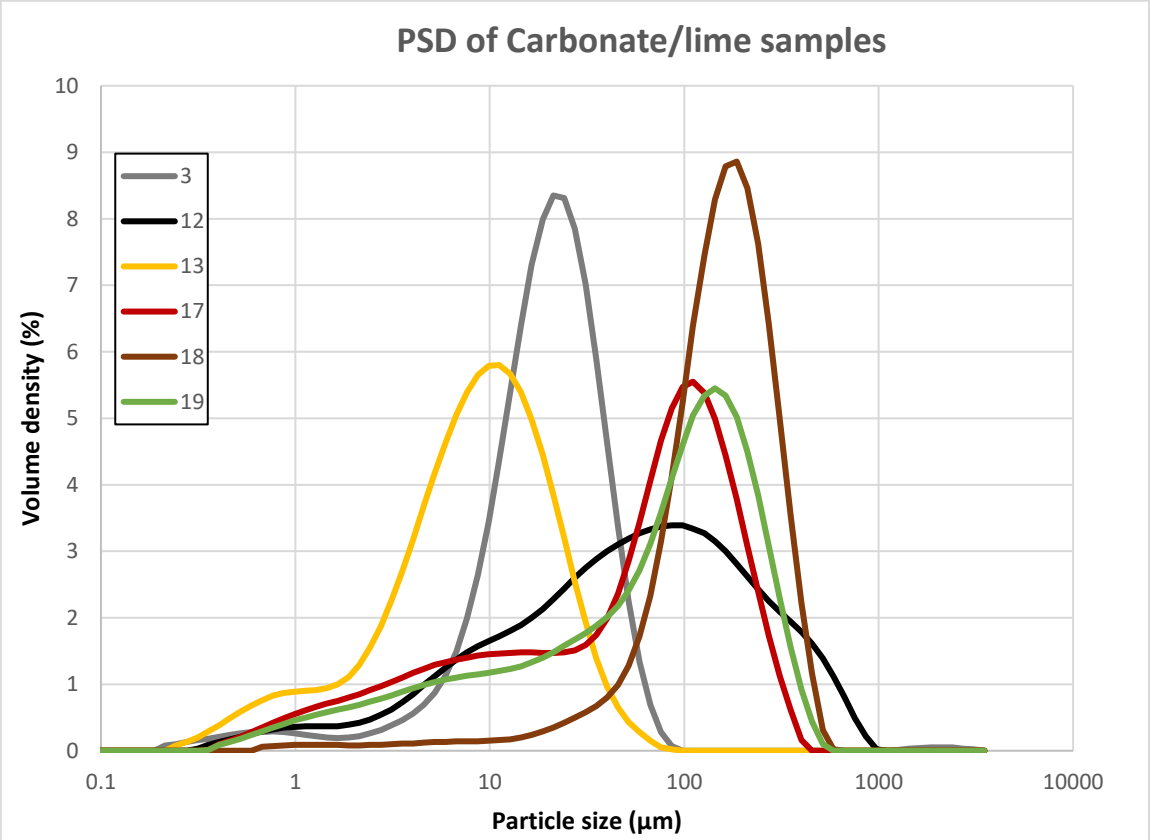

Figure 21. Volumetric particle size distributions of carbonate/lime samples. Operating procedure: stirrer speed of 2500 rpm, analysis time of 15 s and obscuration between 5-15%.

The values of D (10), D (50), D (90) percentiles and volume and surface area means were also obtained with this method. The overall results are represented in Table 4.

Table 4. Derived results from particle size measurements of the carbonate/lime samples

	Particle size, µm				
Sample No.	**D (10)**	**D (50)**	**D (90)**	**D [4;3]**	**D [3;2]**
3	7.5	21.3	43.5	29.8	8.5
12	6	61.5	339	124	11.7
13	1.9	9.3	25.7	12.1	4.1
17	3.6	72.6	205	88.9	9.6
18	64	169	328	184	57.2
19	4.6	90.8	258	113	11.5

Frequency distribution curves of samples #3 and 18 show the similar trend in which both samples have single-peak and the modal diameter, the most commonly occurring diameter of each one, is approximately 25 and 186 µm, respectively (close to their D (50) values). While sample #3 has particle size changing in range of nearly 0.2-90 µm, coarse fraction of tailings from carbonate mine (sample #18) has particle size between about 0.6-600 µm where only 10 % of the population is finer than 64 µm. From the distribution width of sample 12, it can be said that although 90% of the particles are smaller than 340 µm, 10% of the sample consists of particles between 340 µm and 1 mm size. In addition, samples #13, 17 and 19 can be evaluated together since they share similar distributional trend where the frequency of fine particles increase at first and then it follows uniform distribution curve. D [3; 2] values of these samples also show that the particles are quite fine compared to others, especially, the size of particles in lime kiln dust (#13) is very fine where half of the population is smaller than approximately 10 µm and the other half goes up to 86 microns.

The remaining six samples have been categorized together as is shown in Fig. 22 where samples 2 and 6 stand for green liquor dregs, 8a/b for coating sludge, 10 for deinking flotation reject foam and 22 for construction waste. Except for sample 8b (coating sludge), the other samples are polydispersed. According to the results, particle size of sample 8b is in 0.4-500 µm range where 90% of particles in that sample are finer than 35 µm.

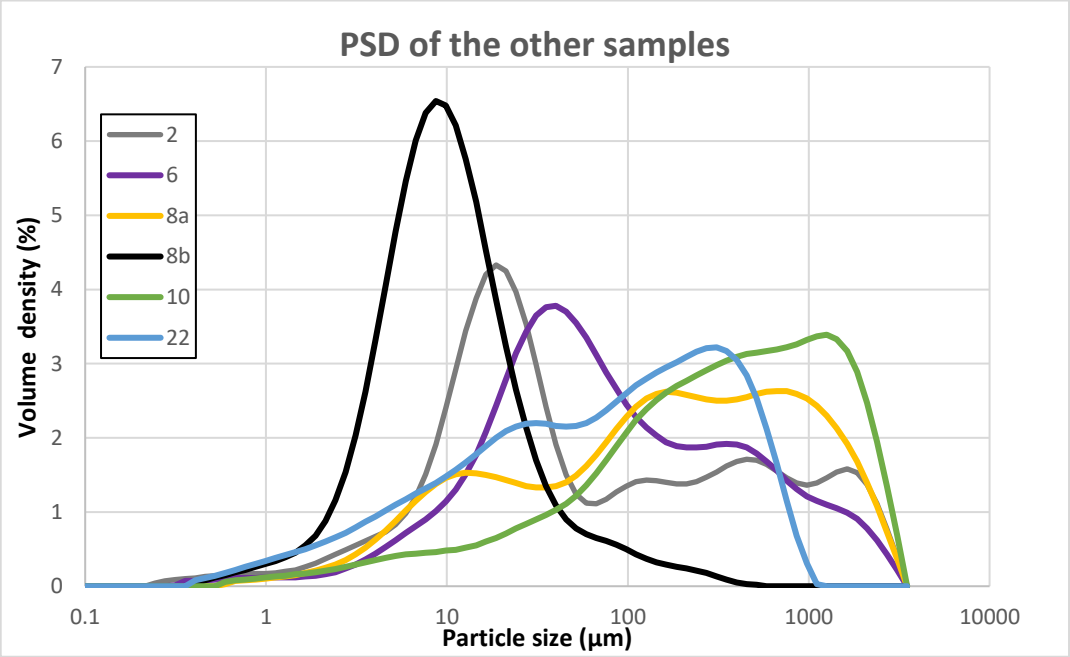

Figure 22. Volumetric particle size distributions of remaining samples. Operating procedure: stirrer speed at 2500 rpm, analysis time of 15 s and obscuration between 5-15%.

The values of D (10), D (50), D (90) percentiles and volume D [4;3] and surface area D [3;2] means were also obtained with this method. The overall results are represented in Table 5.

Table 5. Derived results from particle size measurements of the remaining six samples

	Particle size, µm				
Sample No.	**D (10)**	**D (50)**	**D (90)**	**D [4;3]**	**D [3;2]**
2	8	37.6	1230	345	12.9
6	12.4	69.2	841	285	20.9
8a	9.8	185	1380	466	25.8
8b	3.7	10.2	34.7	19.6	6.9
10	26.2	370	1800	667	37.1
22	5.5	84.8	481	173	12.9

The polydispersity of the samples is obvious based on the significant difference of the three percentiles as can be seen in Table 5. There might be a slight chance that multiple laser scattering happened during the analyses due to possible high concentration of particles but since the obscuration levels in all these samples were between 6-7 % so it is not considered to be a measurement error. As the volume frequency of coarse particles increases non-uniformly, it might be the case that the particles are agglomerating in the dispersion or the raw samples itself are notably non-uniform. It is reasonable to conclude that the particle population of the samples in this group is coarser than the particles of ash and carbonate/lime samples. If sample #10 is taken as an example, it could be said that half of the particles is ranging from 400 µm to 2 mm which is quite broad range compared to the samples of other groups. The distribution width is large in most of the samples including sample 8a where particles of 1.5 mm in diameter are present. The width for sample 8a can be calculated as follows:

$$Span = \frac{D_{0.9} - D_{0.1}}{D_{0.5}};$$

and it is equal to 7.4 in this case which is a big number and it shows how far D (10) and D (90) are apart, normalized wi th the midpoint. (Horiba Instruments, 2017)

7.2 Sieving tests

7.2.1 Selection of the amplitude value for sieving

Amplitude might have a significant influence on the PSD of the samples especially in those cases where the sample sticks onto the sieving medium and tends to agglomerate. In order to see the effect of amplitude, 500 g of lime/slaked lime (#12) sample was taken and the sieve sizes were chosen as 2500 µm, 800 µm, 500 µm, 300 µm, 100 µm, 25 µm and a pan (<25 µm) in downward direction. After the sample had been introduced to the uppermost sieve, amplitude was set to be 0.5 mm and the sample was shaken for 5 min with time interval of 30 seconds. This process was continued thrice by increasing the amplitude to 1.4 mm and 2 mm, but the sieve sizes and the sieving time were kept constant. The obtained results are presented in Fig. 23.

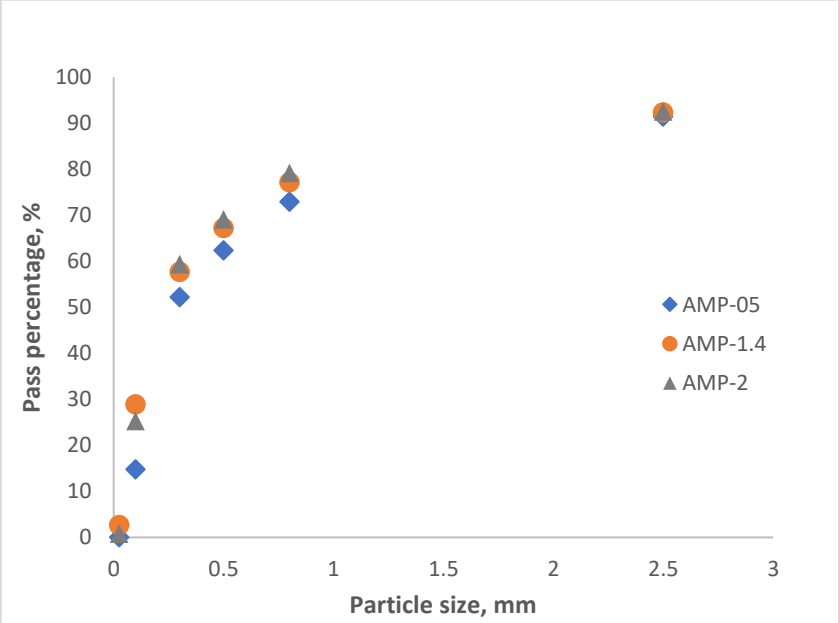

Figure 23. The effect of different amplitudes on sieving results.

As can be seen from the results, pass percentage of sieving is relatively low with the 0.5 mm amplitude which is due to the fact that the particles do not lift off high enough from the sieve bottom to have a chance for orientating freely over the screen medium. Pass percentage in maximum amplitude at 2 mm shows slightly better results than the amplitude value of 1.4 mm but it is not always the case since if particles were thrown too high upwards at high amplitudes, they will have less time to contact with the aperture and pass through it. Although the maximum amplitude (2 mm) gave the best results within 5 minutes experiments, it has not been used in this work since the difference is very slight. Moreover, employing high amplitude might be energy-consuming if sieving will be continued for a long time.

7.2.2 Sieving analysis of raw materials

Sieving analysis was performed by using Haver & Boecker sieve analyser as an alternative to the PSD analysis through laser diffraction method. Different samples whose names were mentioned before were analysed with this method. While laser diffraction analysis gives the number or volume distribution of particles, sieving gives mass distribution of the total particles in any separable size range. The results have been treated in Excel sheet as shown in the example provided in Table 6:

Table 6. An example of how PSD is calculated for one sample in sieving

Sample 11: Ash from gasification on $CaCO_3$ bed					
Sieve opening, µm	Retained wt, g	Differential wt, %	Cumulative wt, g	Cumulative wt, %	Pass percentage, %
2500	33.7	3.37	33.7	3.37	96.63
1250	33.4	3.34	67.1	6.71	93.29
500	251.3	25.12	318.4	31.83	68.17
300	415.9	41.57	734.3	73.40	26.60
100	251.9	25.18	986.2	98.58	1.42
50	5.3	0.53	991.5	99.11	0.89
25	0.4	0.04	991.9	99.15	0.85
Pan	0.3	0.03	992.2	99.18	0.82
Total	992.2				

The amount of the feed sample was 1000.4 g in the beginning and 8.2 g material loss has been observed when the sieving is complete after 70 min of shaking. For this issue, pass percentage of pan is calculated by substracting cumulative weight percentage of pan (99.18%) from 100% which was 0.82% while it was supposed to be 0%. Material loss is inevitable during mechanical sieving; however, the experimental result is valid if the error is in 1-2% range. Differential mass distribution curve represents the retained mass of certain size of particles in different sieves by weight percentage whilst cumulative mass fraction curve gives total amount of retained particles smaller than certain size which is plotted against that size. Differential size distribution is compared for the same sample for sieving and laser diffraction (LD) as in Fig 24.

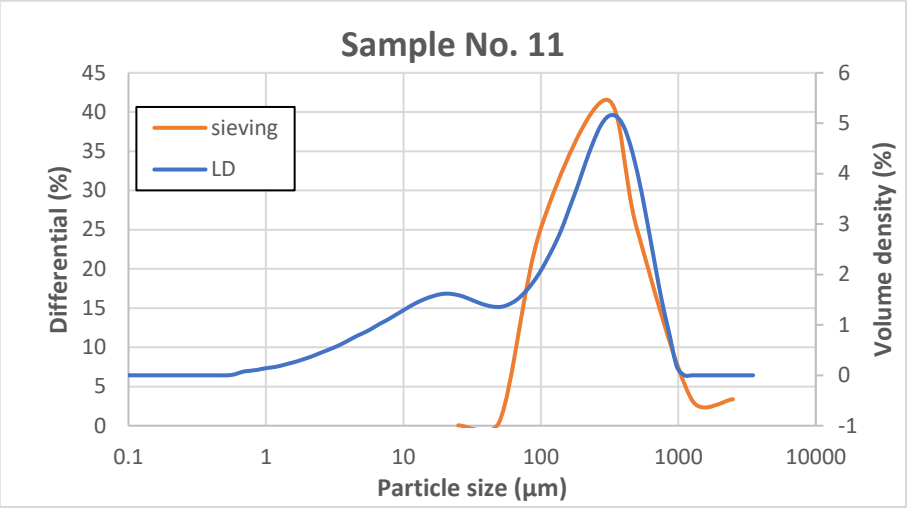

Figure 24. Particle size distribution – ash from gasification on $CaCO_3$ bed (By sieving and Mastersizer 3000)

Although the distribution data presented for LD is volume based and for sieving, it is mass based, the obtained results are quite matching. It can be observed that sieving is more suitable method to analyse coarse particles and laser diffraction is the most appropriate method for fine particulates. As can be seen from Fig. 24, LD can analyse particles smaller than 25 microns while sieving cannot. Such calculations have been made for all the sieved samples and the results will be given based on their cumulative percentages in the next chapter.

7.3 Comparison of sieving and laser diffraction results of raw samples

As in Chapter 8.1, here also ash samples have been categorised together. In Fig. 25, comparison between the PSD results obtained from laser diffraction technique and sieving was carried out for the original raw samples. It is obvious that the particles of ash sample from bark combustion (#1) and fly ash of biomass power plant (#7) are finer than the ash sample from gasification of bark on $CaCO_3$ bed (#11). The aperture size of the sieves was selected separately for each sample before starting the experiment. The chosen sieve sizes and pass/retained percentages of the analysed samples can be found in Appendix 2 in detail.

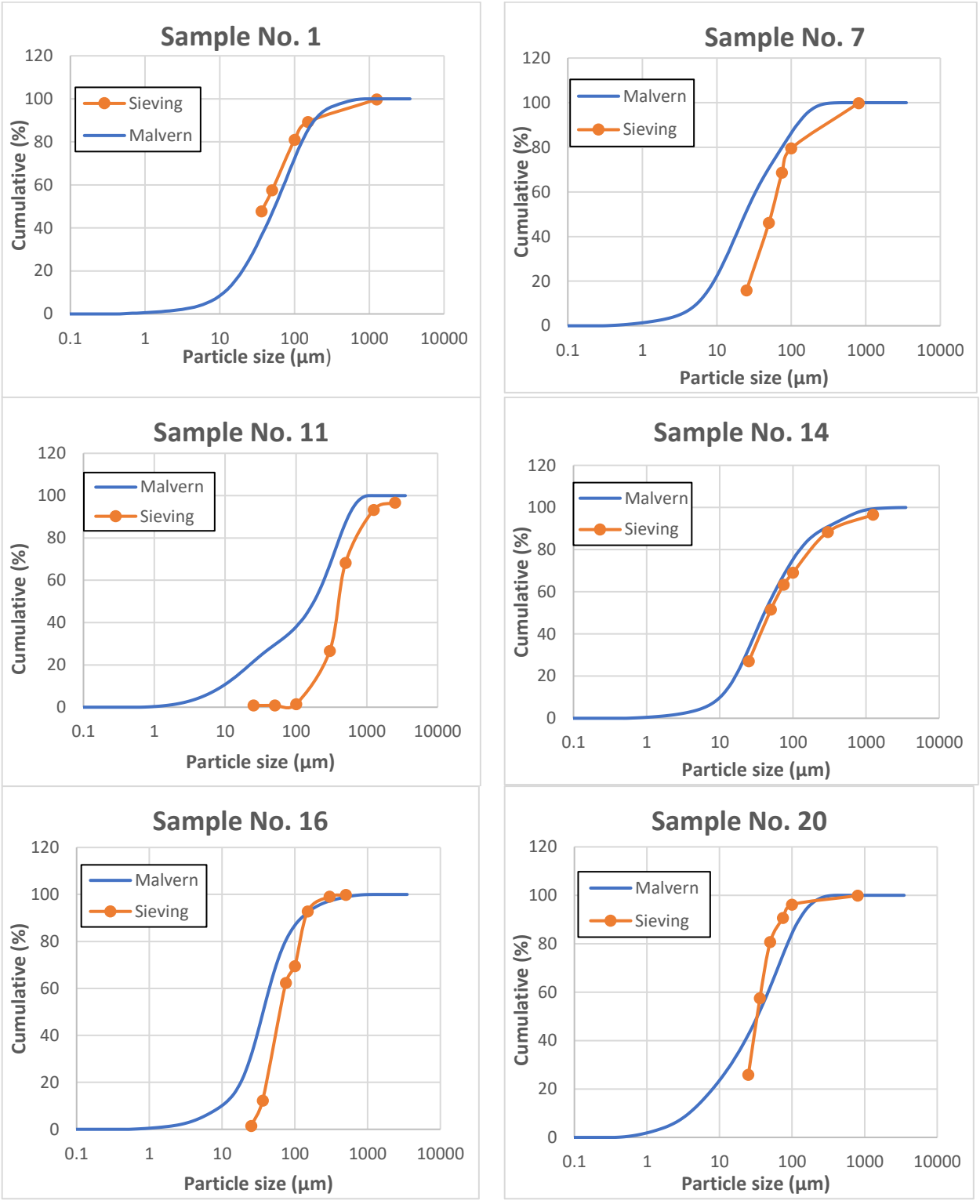

Figure 25. Comparison of sieving and LD results. Sample 1-ash (bark combustion), no. 7-fly ash (biomass power plant), no. 11-ash (gasification of bark on $CaCO_3$ bed), no. 14-fly ash (peat+biomass), no. 16-ash (combustion of bark), no. 20-fly ash (coal).

Although making full comparison between sieve analysis and laser diffraction would not be accurate due to the different based cumulative percentage obtained, some information can be extracted from Fig. 25. While laser diffraction method assumes particles to be spherical and it gives the equivalent diameter of sphere, sieve analysis gives maximum diameter of a sphere that passes through a particular size of a sieve mesh. Ash sample from bark combustion (#1) shows a good correlation with two methods as it can be due to the particles being spherical or close to spherical shape. For fly ash (#7), the particles retained in 800 microns aperture size of sieves are irregularly shaped and tend to agglomerate during sieving, therefore, there is noticeable deviation between the results.

Particle population of the ash sample which is obtained from gasification of bark on $CaCO_3$ bed (#11) is polydisperse and includes particles bigger than 2.5 mm. These seem to be friable charcoal particles of acicular, elongated and irregular shape. Deviation from the two analysis results could arise from particle shapes. For instance, if the particles could pass through the 2.5 mm sieve, their actual size might be $\sqrt{2}$ times of 2.5 which is 3.54 mm. The reason why this assumption has been made is that particle size distribution is highly dependent on the particle orientation where particle can pass the sieve opening diagonally. In some cases, the breadth of a particle passing through the sieve can be even bigger than the diagonal length of sieve aperture. Deviation between the two results may be caused from abovementioned reason as sample #11 contains elongated particulates, too. While these particles were analysed with sieving, they were not dispersed for LD analysis due to the size limitation of the machine and also due to the reason that they float in the dispersion and might not give correct results.

For samples #14, 16 and 20, the two measurement results seem not to differ much, although it has been referred in the study of Hrncirova et al. (2013) that sieving gives inaccurate results for ash samples as they tend to stick together and break up significantly during sieving and they might also dissolve when suspended in water as a dispersion liquid in laser diffraction technique. During sieving, it was observed that the particles of sample #16 were somewhat electrically charged. Although both techniques gave similar results, laser diffraction can analyse finer samples more precisely while for sieving these fine particles are collected in the pan where it can only be said that they are smaller than 25 μm. There are no sieve sizes smaller than 25 microns available for dry sieving due to limitations caused by surface charges. Normally, dry particles finer than 25 μm are agglomerated due to fairly high adhesion forces.

Carbonate and lime-based samples have been categorized together as can be seen in Fig. 26. Although cumulative percentage of laser diffraction is volume-based and sieving results represent mass-based cumulative percentages, the trends of the curves can be compared. Samples #3, 12 and 13 from kraft pulp mills were dried before sieving since they had high moisture content.

During drying, particles of these samples, especially sample #12 formed big agglomerates, therefore they were carefully crushed before sieving. This might be one of the explanations for the deviation between the results. In top sieve fraction of sample #12, particles bigger than 2.5 mm diameter were present with rounded shape. The particles of samples 3 and 13 were fine which should not cause difficulty in dispersion of the sample for laser diffraction method; the sieving of these samples was repeated twice in order to obtain representative results. Despite the fact that sieving has been carried out for 80 min and 60 min for samples 3 and 13, respectively with 1.5 and 1.2 mm amplitude of shaking, effective fractionation could not be achieved due to sieve blinding since the samples were sticking on the sieve medium.

Comparison between the results of samples #17 and 18 gave desirable correlation. Tailings from fine fraction of carbonate mine (#17) formed agglomerates after drying which then were broken and sieved for 60 min in total. Sieving was interrupted after some time for weighing the fractions, as it was the case for all the samples to make sure of the end point. Besides that, aggregates have been observed during shaking period and they were broken in back-weighing time. Coarse fraction of tailings (#18) has the closest values with laser diffraction results. Although the cumulative percentages are volume and mass based and it is not convertible as the density of the sample is not known, it is possible to say that the shape of real particles were close to spherical.

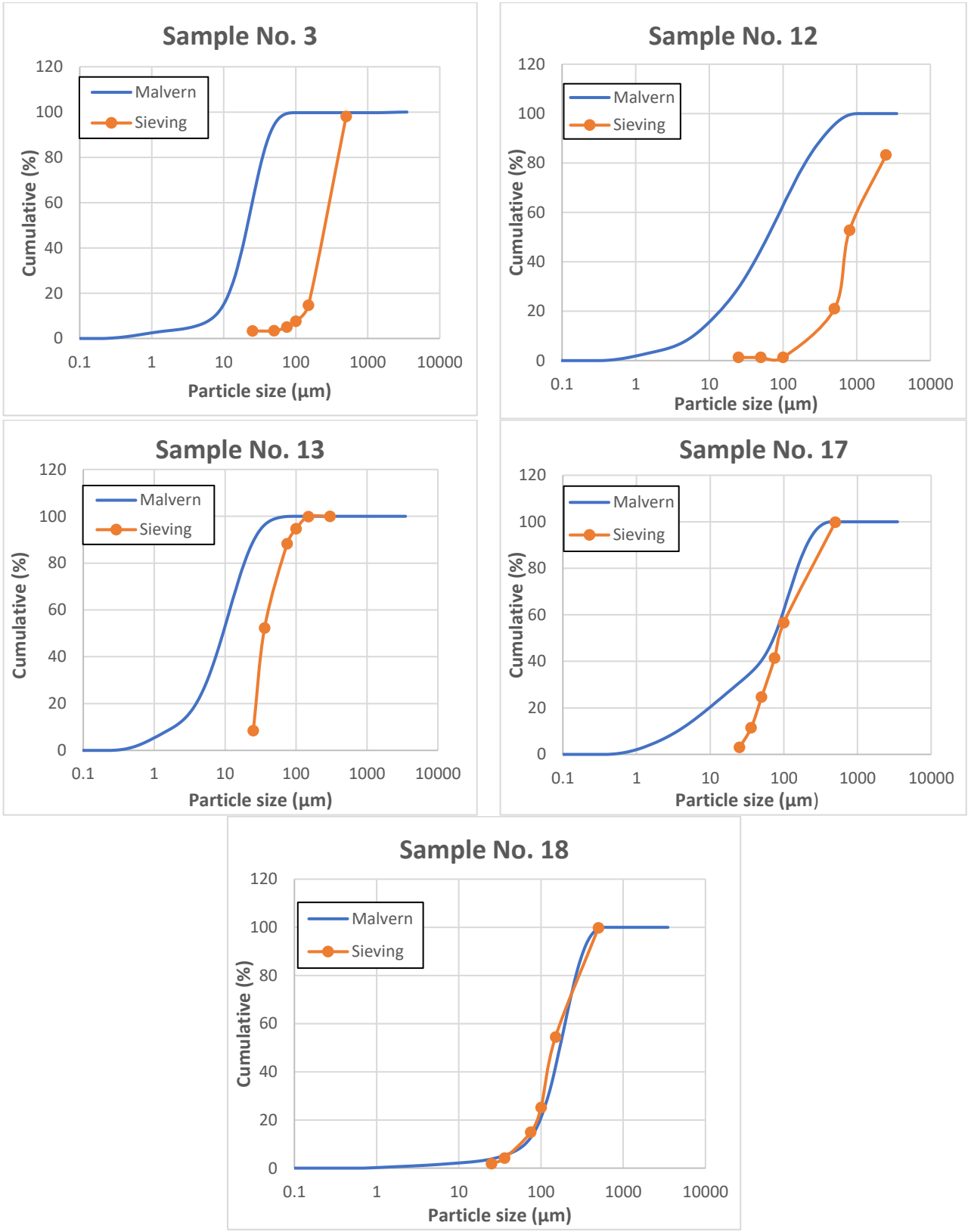

Figure 26. Comparison of sieving and LD results. Sample 3-$CaCO_3$ (from chemical recovery cycle), no. 12-lime/slaked lime, no. 13-lime kiln dust, no. 17-tailings, fine fraction (from carbonate mine), no. 18-tailings, coarse fraction (from carbonate mine)

Bottom ash from co-incineration (#5) and sample of construction waste (#22) are presented in Fig. 27. Some 'needle-like' and irregularly shaped particles have been manually removed from sample 5 before sieving, but their weight was added to the weight of the retained fraction of the top sieve. Since the particles were very coarse in this sample, it was decided not to determine the PSD via Mastersizer 3000 as it could have damaged the equipment. However, the sieve fractions smaller than 800 microns size were analysed via LD to determine the median shift on the fractions which will be also explained.

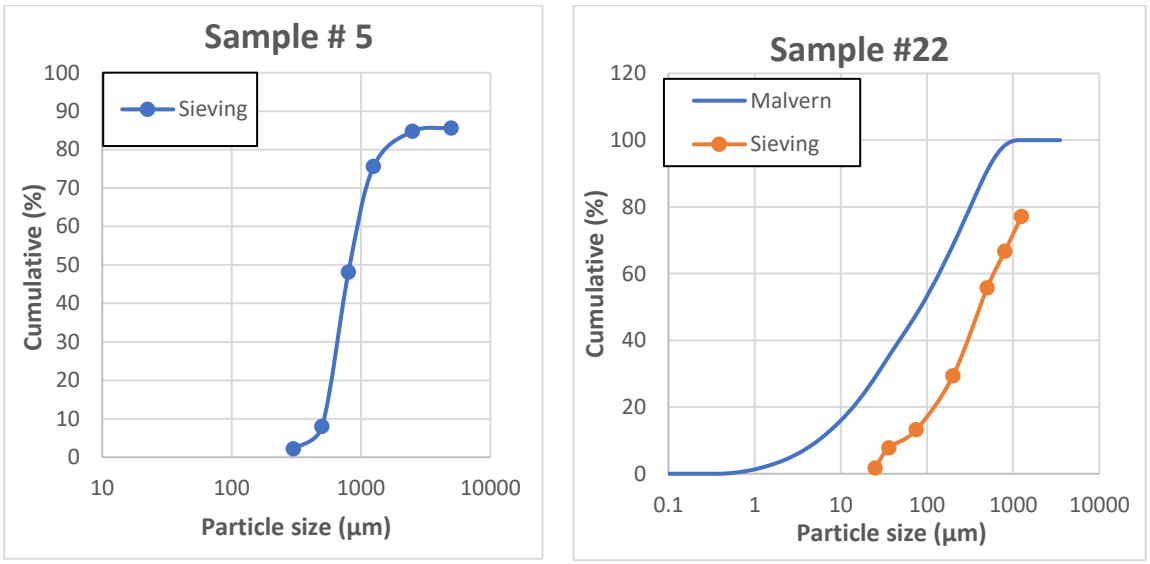

Figure 27. Comparison of sieving and LD results. Sample 5-bottom ash (co-incineration), no. 22-construction waste

Sample 22 is a construction waste that contains particles above 1.25 mm down to 1 µm. The employed sieve sizes can be found in Appendix 2. Correlation is poor between the results which can be explained by the shapes of particles as sieving allows one to observe particles with naked eye. The fractions of 1.25 mm, 800 µm and 500 µm sieves are irregularly shaped including some glass pieces and rounded particles. When the sub-samples from 200 µm and other downward sieves were collected, it was observed that fractions from 200 µm and 36 µm sieve sizes include some particles in the form of 'fibre'. Since the particles were not spherical as assumed in laser diffraction method, the reason behind the deviation of results from both techniques is understandable.

7.4 PSD measurements of fractionated sub-samples by Mastersizer 3000

Sieving analysis classified the samples to different size fractions. The fractionated sub-samples were then collected in the sample bottles for further analysis. There were some cases that representative samples could not be collected, therefore, they were not analysed. For instance, this occurred in the cases where the pass percentage of the selected sieve size was almost 100% and left only small amount of retained sample in the upper sieve or when the sample was mostly retained on the top sieves and only small amount had passed through the downward sieve. In other cases, particles of raw material or sub-samples of sieve fractions were so coarse that their particle size was out of the measurement range of Malvern Mastersizer 3000. Other than these, 83 samples altogether from sieve fractions, including raw samples were analysed by the laser diffraction method.

Although sieving serves to separate coarse particles from fine ones, it is almost always a case that contamination by fines exists in the coarser fractions and vice versa. From Fig. 28, effective separation can be seen in the example of samples #14.

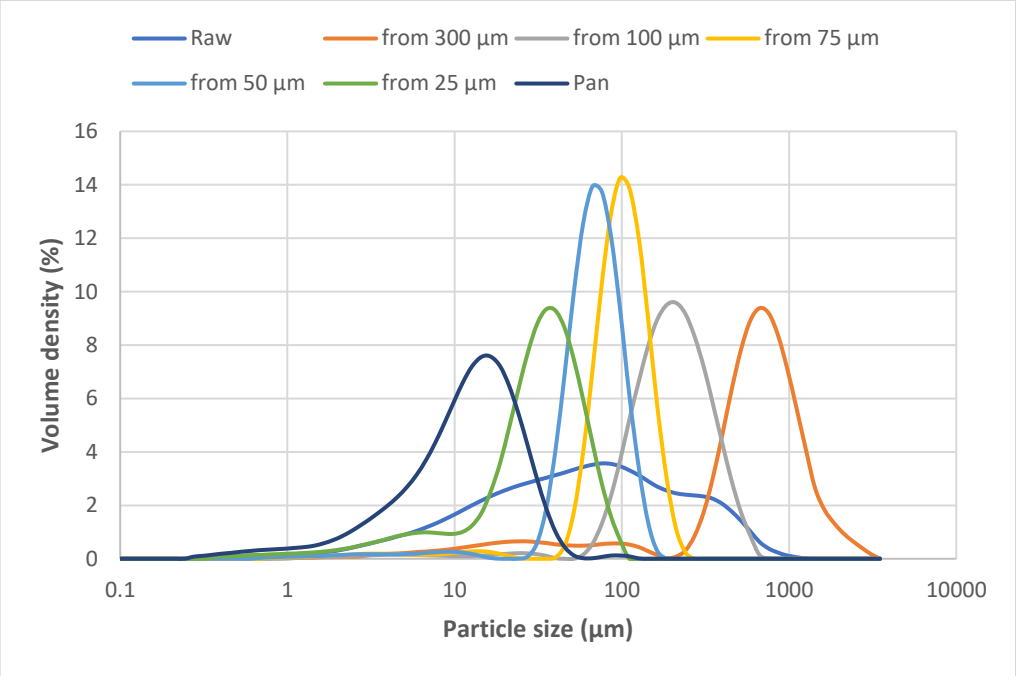

Figure 28. PSD measurements of fractionated sub-samples of sample #14

Sample #14 contains fly ash from combustion of peat and biomass mixture. The sieves were chosen as aperture sizes of 300 µm, 100 µm, 75 µm, 50 µm, 25 µm and pan in downward direction. When the sample fractions were analysed by the laser diffraction method, it was observed that, for instance, D (50) value of the fractions retained in 50 µm

sieve was 74 µm which is reasonable as this sieve rejects particles below 100 µm and above 50 µm. Median shifts for all sub-samples are reasonable for sample #14, however, the separation is not perfect. It would be an ideal fractionation when the underflow did not contain particles larger than the cut size and vice versa and the distribution curves did not overlap when the median shifts to the finer sizes.

Similarly, median shift was checked for sample #3 (Fig. 29) which was $CaCO_3$ sample from chemical recovery cycle of a kraft pulp mill. The stack of test sieves was selected with aperture sizes of 150 µm, 100 µm, 75 µm, 50 µm and 25 µm and pan in the bottom. Since there was no collected representative sample in the sieve size of 25 µm and pan (See Appendix 2), their PSDs are not included in Fig. 29. Since the particles are so fine and selected sieve sizes are very close to each other, median shift cannot be seen as sharply as in sample #14. These results show in what extent the sieving analysis was effective and provides all other available data extracted from Mastersizer 3000. To summarise, it can presumably be said that sieving was not very effective for sample #3 if this result is compared with the graph of sample #3 in Fig 26. Poor separation might be caused from the sample stickiness (See Appendix 3 for other samples).

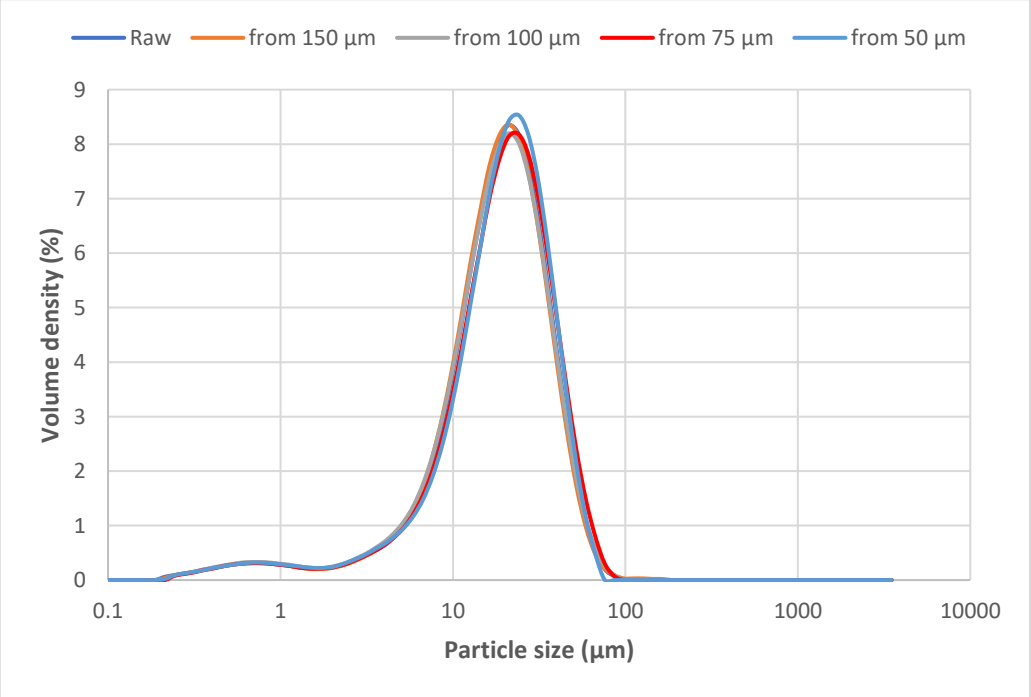

Figure 29. PSD measurements of fractionated sub-samples of sample #3

7.5 Color differences of sieved fractions

After the individual sieve fractions were placed side by side, it was observed that there is discernible color differences in the fractions of some samples, such as samples #1, 14 and 16 which are all ash samples. In Fig. 30, different sieve fractions of sample 1 are presented.

Figure 30. Fractions from sieving of sample 1 (ash from combustion process of bark). Raw sample (a), 1250 µm (b), 150 µm (c), 100 µm (d), 50 µm (e), 36 µm (f)

As this ash sample is obtained from the combustion of biomass (bark), the ash content can be predicted based on the carbohydrate structure of the biomass. From the literature, it is obvious that major elements of the biomass (depending if the species are originating from hardwood or softwood) are C, H, O, N, Si, K, Ca, Al, Fe and even some heavy metals can be added to this list (Michalik & Wilczynska-Michalik, 2012). When the bark is combusted, various components can be formed due to the complex reactions depending on the fuel type, moisture content, applied temperature, amount of impurities and some other factors. The bark contains some impurities, such as soil and sand in this case. Also, when the inorganic species are combusted, there might be SiO_2, Al_2O_3, CaO and Fe_2O_3 formed as a

result of oxidation reactions and some hydrocarbons will be formed also from the combustion of organic species.

It can be assumed that the fraction from 1250 µm aperture width displays black color attributable to its high C (carbon) content (Fig. 30 (b)). As it comes to lower fractions, high C content is still present but with smaller particle size (150 µm). Although the color change is not as sharp in the rest of the fractions, it is still apparent that the chemical composition of these sub-samples differs from each other which could be confirmed by chemical analysis to find their exact ash contents. Since the color changes from very black tone to relatively lighter towards the finer fractions, it can be said that C content starts to decrease while the amount of SiO_2, Al_2O_3 or other inorganic components increase.

8 Conclusions

This work has outlined the comparison between the results obtained from two different particle size analysis techniques of the industrial solid side streams. These techniques include laser diffraction (LD) method which was carried out by using Mastersizer 3000 equipment and sieving with Haver & Boecker sieve shaker. The raw materials were mostly ash samples from different processes, green liquor dregs, tailings, lime mud consisting mainly of $CaCO_3$, coating sludge, deinking flotation reject foam, lime and construction waste. Although there were a few samples of the similar type, they varied from one another in terms of their particle sizes since those samples were obtained from different processes or different companies. Altogether PSD of 19 samples was analysed by Mastersizer 3000 and 13 of them were analysed also by sieving. The sub-samples fractionated from sieving process (83 subsamples) were then analysed by the LD method to check the median shift and separation efficiency of the sieving.

In order to start measuring the PSD of raw materials, some experiments were carried out to find appropriate values of operating parameters. For LD analyses, Fraunhofer optical model was used with water as the dispersion medium, as the samples were not soluble in water. Afterwards, other parameters including measurement time, ultrasonication effect, stirring speed and obscuration level were selected and those parameters were used as the reference in the determination of the PSD of raw samples. Moreover, optimal amplitude value was selected for the sieving method.

The length of measurement time for the LD analysis was selected by observing the change in Sauter mean diameter during 5 s, 10 s, 15 s and 30 s periods. It was assumed from the results that 5 s and 10 s might be too short to represent all sizes of the aliquot in the dispersion and 30 s might be too long since some samples continued becoming finer by time. Therefore, 15 s seems to be reasonable to use for further measurements. Similarly, 50% of US treatment with 60 s was introduced to the system and the percentiles were recorded before, during and after US treatment. D (90) value of the sample was used as a response to this and since the influence of US stayed somewhat dubious, it was decided not to apply US in the analysis of raw samples. Another parameter to be analyzed was stirrer speed which was applied in the range 1000-3500 rpm with 500 rpm increments and the changes in three percentiles were checked. Although the decile, D (90), showed significant increase with the increment of the stirrer speed, it has been decided to go for 2500 rpm because the high impeller speed somewhat might lower homogeneity of the suspension. Obscuration was a parameter which can also have impact on the obtained data, because the lower value of it may result in insufficient number of snapshots and higher value may lead to multiple scattering. This value has been changed to 3%, 9%, 14% and 19% to check the frequency-based PSD and 14% seemed to be a reasonable value. In the experiments, the obscuration level has been in 5-15% interval. In the sieving method, sieving time was not decided initially as each sample had a different end point. So, the only adjustable parameter was amplitude which was selected by experimenting sample 12 for 5 minutes. Each analysis was conducted in 0.5 mm, 1.4 mm and 2 mm amplitude values and 1.4 mm was selected to be used because it is not too high to float the particles by decreasing their contacts with sieve apertures and not too low to prevent lifting off particles.

Since the samples 2, 6, 8, 10 and 19 were in slurry form, they were only analyzed with LD and PSD of sample #5 was only analyzed by sieving as it was too coarse. The rest 13 samples were analyzed by both techniques. Even though direct comparison is not valid between methods, the results were compared in terms of their cumulative mass and volume based percentages. Very poor correlation existed when the particles were acicular, elongated, rods or irregularly shaped. Moreover, while $CaCO_3$ (sample #3), lime/slaked lime (#12) and lime kiln dust (#13) were sieved, sieve blinding took place due to the stickiness of the samples. Usage of LD method in size distribution determination of such samples seems to be more appropriate for analysis rather than sieving. It is proved by the LD experiments of fractionated sub-samples where medium shifts were studied and found that there is a big overlap in medians of different sieve size fractions which could arise from poor sieving performance.

This work has outlined that sieving analysis does not always give ideal results for particle sizing of every sample. Especially, when the sample to be sieved is sticky, tends to agglomerate or is electrostatically charged, it is difficult to obtain reliable results. Despite this it is very effective in ash samples and neutral samples, such as soil or construction material and it still remains as a preferred choice in industries since it can analyze broad size range of particles. In addition, LD measurements do not always give reliable results, in particular when the particles are friable, irregularly shaped and coarse.

It is believed that there is no one universal method for determination of PSD of samples, especially of polydisperse samples, because all available methods, no matter traditional or new, still have some inherent flaws. The choice between the methods needs to be considered according to their balance between the pros and cons of each. Nowadays, the speed, reproducibility, range of available output options, small amount of required sample and robustness make LD technique much more attractive in determination of PSD and these features provide precise and rapid results. Despite the advantages outlined above, it is not accurate as the response to each particle depends on its alignment and repeated experiments can give different size distributions for the same sample. Sieving also has some advantages over LD method; most importantly, it is reliable in the analysis of coarse particles and allows its user to see the particle shape and the color change in case it happens between the fractions of the same sample. In addition, it provides one with the cumulative or differential mass percentage of the particles which is very important to know for further utilization. For instance, if the mass of a certain size of particles retained in the sieve is very low, it might be unsuitable for large scale utilization. Besides, sieving has some limitations, such as the drawback that a non-spherical particle can pass through or retain on a given mesh size of sieve depending on its shape and orientation and due to sieve blinding problem.

It can be concluded that different instruments give equally ‘correct’ results but each instrument may represent its ‘correct’ results in its own terms and each yields only estimations of PSD. However, it can be concluded that PSD measurement is much more reliable if the analyses of LD and sieving are combined together as it is carried out in this work which would give extensive and more accurate information about the real particle size of the sample. While sieving can measure coarse particles, LD measures fine particles down to microns and they complete each other in this regard. Additionally, while a raw sample cannot be analyzed by LD due to the presence of very large particles, its fractions

within the sizing range of LD can be studied after sieving, which once more proves that the combination of both methods is more reliable.

References

Abdollahzadeh, L., Habibian, M., Etezazian, R. & Naseri, S., 2015. Study of particle's shape factor, inlet velocity and feed concentration on mini-hydrocyclone classification and fishhook effect. *Powder Technology,* Volume 283, pp. 294-301.

Abdulmatin, A., Tangchirapat, W. & Jaturapitakkul, C., 2017. Environmentally friendly interlocking concrete paving block containing new cementing material and recycled concrete aggregate. *European Journal of Environmental and Civil Engineering,* pp. 1-18.

Allen, T., 2003. *Powder Sampling and Particle Size Determination.* 1st ed. Amsterdam: Elsevier.

Andersson, R., 2010. *Evaluation of two hydrocyclone designs for pulp fractionation,* Stockholm: s.n.

Anon (a), 2005. *How to carry out Wet Sieving,* Haan, Germany: Retsch GmbH.

Anon (b), 2012. *The gas cyclone,* Chemnitz, Germany: Suviz GmbH.

Augusto, P. A. et al., 2017. Method to evaluate and prove-the-concept of magnetic separation and/or classification of particles. *Journal of Magnetism and Magnetic Materials,* pp. 405-414.

Backhurst, J. R., 1991. Particle technology & Separation Process. In: J. F. Richardson & J. H. Harker, eds. *Coulson & Richardson's Chemical Engineering.* Oxford: Pergamon Press, pp. 1-13.

Badur, S. & Chaudhary, R., 2008. Utilization of hazardous wastes and by-products as a green concrete material through s/s process: A review. *Advanced Study Center Co. Ltd,* Volume 17, pp. 42-61.

Barbosa-Canovas, G., Ortega-Rivas, E., Juliano, P. & Yan, H., 2005. *Food powders: Physical properties, Processing and Functionality.* New York: Kluwer Academic/Plenum Publishers.

Berry, M., Cross, D. & Stephens, J., 2009. *Changing the environment: An alternative "green" concrete produced without Portland cement.* Lexington, World of Coal Ash (WOCA) conference.

Boschetto, A. & Giordano, V., 2012. Powder sampling and characterization by digital image analysis. *Measurement,* 45(5), pp. 1023-1038.

Bourgeois, F. & Majumder, A. K., 2013. Is the fish-hook effect in hydrocyclones a real phenomenon?. *Powder Technology,* Volume 237, pp. 367-375.

Bowen, P., 2002. Particle Size Distribution Measurement from Millimeters to Nanometers and from Rods to Platelets. *Journal of Dispersion Science and Technology,* 23(5), pp. 631-662.

Brittain, H. J., 2002. Particle-Size Distribution, Part III. *Determination by Analytical sieving*.

Cepuritis, R. et al., 2017. Measurement of particle size distribution and specific surface area for crushed concrete aggregate fines. *Advanced Powder Technology,* 28(3), pp. 706-720.

Cho, H. . C. & Kim, J. K., 1999. Analysis on the Efficiency of the Air Classification of Fly Ash. *Geosystem Engineering,* 2(2), pp. 37-42.

Cohen, H. E., 2012. Ulmann's Encyclopedia of Industrial Chemistry. In: *Solid–Solid Separation, Introduction.* Weinheim: Wiley-VCH Verlag GmbH & Co, pp. 597-603.

Di Stefano, C., Ferro, V. & Mirabile, S., 2010. Comparison between grain-size analyses using laser diffraction and sedimentation methods. *Biosystem Engineering,* 106(2), pp. 205-215.

Edwards, P., 2017. *Global Cement Top 100 Report 2017 - 2018,* s.l.: Global Cement Magazine.

Ferro, V. & Mirabile, S., 2009. Comparing particle size distribution analysis by sedimentation and laser diffraction method. *Agroengineering,* Volume 2, pp. 35-43.

Fisher, G. L. et al., 1978. Physical and Morphological Studies of Size-Classified Coal Fly Ash. *Environmental Science & Technology,* 12(4), pp. 447-451.

Freeman, T., 2014. *An Introduction to Powders,* Gloucestershire, UK: Freemantechnology.

Gawali, S. W. & Bhambere, M. B., 2015. Effect of design and the operating parameters on the performance of cyclone separator-a review. *International Journal of Mechanical Engineering and Robotics Research,* 4(1).

Golmaei, M., Kinnarinen, T., Jernström, E. & Häkkinen, A., 2018. Efficient separation of hazardous trace metals and improvement of the filtration properties of green liquor dregs by a hydrocyclone. *Journal of Cleaner Production,* Volume 183, pp. 162-171.

Grewal, I., 2018. *Mineral Processing Introduction,* Langley, Canada: Met-solve laboratories inc..

Hassellöv, M. et al., 2001. Particle Size Distributions of Clay-rich Sediments and Pure Clay Minerals: A Comparison of Grain Size Analysis with Sedimentation Field-Flow Fractionation. *Aquatic Geochemistry,* Volume 7, pp. 155-171.

Heiskanen, K., 1987. *Classification Handbook.* Lappeenranta: Etelä-Saimaan Kustannus Oy .

Hogg, R., Turek, M. L. & Kaya, E., 2004. The Role of Particle Shape in Size Analysis and the Evaluation of Comminution Processes. *Particulate Science and Technology,* 22(4), pp. 355-366.

Horiba Instruments, 2017. *A Guidebook to Particle Size Anlysis,* Irvine, USA: Horiba Instruments, INC.

Hrncirova, M., Pospisil, J. & Spilacek, M., 2013. Size analysis of solid particles using laser diffraction and sieving analysis. *Engineering Mechanics,* Volume 20, pp. 309-318.

Huseynov, E., Garibov, A. & Mehdiyeva, R., 2016. TEM and SEM study of nano SiO2 particles exposed to influence of neutron flux. *Journal of Materials Research and Technology,* 5(3), pp. 213-218.

Johansson, R., 2014. *Air classification of fine aggregates (Doctoral dissertation),* Göteborg, Sweden: Chalmers University of Technology.

Kashiwaya, K. et al., 2012. Effect of particle shape on hydrocyclone classification. *Powder Technology,* Volume 226, pp. 147-156.

Kippax, P., 2005. *Measuring Particle Size: Using Modern Laser Diffraction Techniques.* s.l., Paint & Coating Industry Magazine.

Mäkitalo, M., Maurice, C., Jia, Y. & Öhlander, B., 2014. Characterization of green liquor dregs, potentially useful for prevention of the formation of acid rock drainage. *Minerals,* Volume 4, pp. 330-344.

Malvern Instruments Ltd, 2013. *Wet or Liquid Dispersion Method Development for Laser Diffraction Particle Size Measurements,* Worcestershire, UK: Malvern.

Malvern Panalytical, 2018. *Image analysis,* Worcestershire, UK: Malvern Panalytical Ltd.

Masuda, H., Higashitani, K. & Yoshida, H., 2006. *Powder Technology Handbook.* 3rd ed. Boca raton, Florida: RC Press.

Matsuyama, T. & Yamamoto, H., 2005. Particle Shape and Laser Diffraction: A Discussion of the Particle Shape Problem. *Journal of Dispersion Science and Technology,* 25(4), pp. 409-416.

Merkus, H. G., 2009. Particle size measurements. In: *Electrical Sensing Zone.* s.l.:Springer Science+Business Media B.V., pp. 241-256.

Merkus, H. G., 2009. *Particle Size Measurements; Fundamentals, Practice, Quality.* The Netherlands: Springer.

Michalik, M. & Wilczynska-Michalik, W., 2012. Mineral and chemical composition of biomass ash. *European Mineralogical Conference,* Volume 1.

Micrometrics, 2000. *Micromeritics.* [Online] Available at: http://www.micromeritics.com/Product-Showcase/SediGraph-III-Plus.aspx [Accessed 5/ 4/ 2018].

Morse, P. & Loxley, A., 2009. Light Microscopic Determination of Particle Size Distribution in an Aqueous Gel. *Drug delivery technology,* 9(5).

Nguyen, A. V. & Luo, L., 2016. *A review of principles and applications of magnetic flocculation to separate ultrafine magnetic particles,* s.l.: s.n.

Oberteuffer, J. A., 1974. Magnetic Separation: A Review of Principles, Devices and Applications. *IBEE Transactions on Magnetics,* Volume 10, pp. 223-238.

Ortega-Rivas, E., 2012. Separation Techniques for Solids and Suspensions. In: G. V. Barbosa-Ca´novas, ed. *Non-thermal Food Engineering Operations.* Chihuahua: Springer, Boston, MA, pp. 131-197.

Otwinowski, H., 2013. Cut Size Determination of Centrifugal Classifier with Fluidized Bed. *Archives of Mining Sciences,* 58(3), pp. 823-841.

Patchigolla, K., Wilkinson, D. & Li, M., 2006. Measuring Size Distribution of Organic Crystals of Different Shapes Using Different Technologies. *Part. Part. Syst. Charact. 23 ,* pp. 138-144.

Prakasha, S., Dasa, B., Mohantya, J. & Venugopalb, R., 1999. The recovery of fine iron minerals from quartz and corundum mixtures using selective magnetic coating. *International Journal of Mineral Processing,* 57(2), pp. 87-103.

Retsch Technology, 2018. *Particle Size and Particle Shape Analysis,* Haan, Germany: Retsch Technology GmbH.

Saravacos, G. & Kostaropoulos, A. E., 2016. *Handbook of Food Processing Equipment.* 2nd ed. Athens, Greece: Springer.

Schmidt, J. & Werther, J., 2006. Simulation and optimization of a centrifugal fluidized bed classifier in the micrometer range. *Chemical Engineering and Processing: Process Intensification,* 45(6), pp. 488-499.

Shapiro, M. & Galperin, V., 2005. Air classification of solid particles: a review. *Chemical Engineering and Processing: Process Intensification,* 44(2), pp. 279-285.

Su, D., 2017. Advanced electron microscopy characterization of nanomaterials for catalysis. *Green energy & Environment,* II(2), pp. 70-83.

Svarovsky, L., 2000. *Solid-liquid Separation.* 4th ed. Butterworth/Heinemann: Reed Elsevier.

Tarleton, S., 2015. *Progress in Filtration and Separation.* Loughborough, UK: Elsevier.

Tomas, J., 2012. *Particle separation,* Madgeburg, Germany: MVT media.

Ujam, A. & Enebe, K., 2013. Experimental Analysis of Particle Size Distribution using Electromagnetic Sieve. *American Journal of Engineering Research (AJER),* 02(10), pp. 77-85.

Wang, Guifeng, Tong & Xin, 2011. Screening efficiency and screen length of a linear vibrating screen using DEM 3D simulation. *Mining Science and Technology (China),* 21(3), pp. 451-455.

Wang, J. et al., 2015. The effect of particle density on the sources, distribution, and degradation of sedimentary organic carbon in the Changjiang Estuary and adjacent shelf. *Chemical Geology,* Volume 402, pp. 52-67.

Weber, A. P. & Legenhausen, K., 2014. Characterization of a Classification or Separation Process. *Wiley Online Library.*

Will's, B. A. & Napier-Munn, T., 2006. An introduction to the practical aspects of ore treatment and mineral recovery. In: T. Napier-Munn, ed. *Will's Mineral Processing Technology.* Burlington: Elsevier, pp. 203-223.

Wu, S.-E.et al., 2017. Effectiveness of a hydrocyclone in separating particles suspended in power law fluids. *Powder Technology,* Volume 320, pp. 546-554.

Wynn, E. J. & Hounslow, M. J., 1997. Coincidence correction for electrical-zone (Coulter-counter) particle size analysers. *Powder Tehnology,* 93(2), pp. 163-175.

Yamamoto, T. & Higashino, M., 2016. Effect of the surface properties of particle on the classification performance of a dry-cyclone. *Particulate Science and Technology,* 36(1), pp. 46-49.

Yu, J.-F., Fu, J., Cheng, H. & Cui, Z., 2017. Recycling of rare earth particle by mini-hydrocyclones. *Waste Management,* Volume 61, pp. 362-371.

Zárybnická, M., Pospíšil, J. & Špiláček, M., 2012. Comparison of sieve analysis and laser diffraction for size distribution of fine ash particles. 26 June.

Zhang, X., 2016. *Emission standards and control of PM from coal-fired power plant,* London : IEA Clean Coal Service.

Zhang, Y. et al., 2017. Understanding the separation of particles in a hydrocyclone by force analysis. *Powder Technology,* Volume 322, pp. 471-489.

Appendices

APPENDIX I: Samples numbering, names and their PSD determination methods

No:	Sample	Malvern	Sieving
1	Ash (bark combustion)	✓	✓
2	Green liquor dregs	✓	x
3	$CaCO_3$ (from chemical recovery cycle)	✓	✓
4	Fly ash (co-incineration)	✓	x
5	Bottom ash (co-incineration)	x	✓
6	Green liquor dregs	✓	x
7	Fly ash (biomass power plant)	✓	✓
8	Coating sludge	✓	x
9	Mixed sludge (deinking sludge +biowaste +fiber waste)	x	x
10	Deinking flotation reject foam	✓	x
11	Ash (gasification of bark on $CaCO_3$ bed)	✓	✓
12	Lime/ slaked lime ($CaO/Ca(OH)_2$)	✓	✓
13	Lime kiln dust	✓	✓
14	Fly ash (peat+ biomass)	✓	✓
16	Ash (combustion of bark)	✓	✓
17	Tailings, fine fraction (from carbonate mine)	✓	✓
18	Tailings, coarse fraction (from carbonate mine)	✓	✓
19	Thickening pilot underflow (from carbonate mine)	✓	x
20	Fly ash (coal)	✓	✓
21	Fly ash (municipal waste)	x	x
22	Construction waste	✓	✓

APPENDIX II: Details for sieving experiments; Used sieve sizes and retained/passed amounts with percentage. Raw sample was taken nearly 1 kg for each sample to be sieved, except for samples No. 16 and 22 which weighed 348 g and 460 g, respectively. Shaking was carried out at the amplitude of 1-1.5 mm with the interval time of 30 s.

Appendix II, 1 Sieving results of ash samples No. 1, 5 and 7.

Sample No. 1			Sample No. 5			Sample No. 7		
Sieve opening, μm	**Retained amount, %**	**Passed amount, %**	**Sieve opening, μm**	**Retained amount, %**	**Passed amount, %**	**Sieve opening, μm**	**Retained amount, %**	**Passed amount, %**
1250	0.26	99.74	5000	14.38	85.62	800	0.19	99.81
150	10.55	89.19	2500	0.89	84.73	100	20.28	79.53
100	8.25	80.94	1250	9.17	75.56	75	10.86	68.67
50	23.47	57.47	800	27.78	48.08	50	22.58	46.09
36	9.78	47.7	500	40.06	8.02	25	30.19	15.9
Pan	47.64		300	5.84	2.18	Pan	15.86	
			Pan	2.47				

Appendix II, 2 Sieving results of ash samples No. 11, 14, 16 and 20.

Sample No. 11			Sample No. 14			Sample No. 16			Sample No. 20		
Sieve opening, µm	**Retained amount, %**	**Passed amount, %**	**Sieve opening, µm**	**Retained amount, %**	**Passed amount, %**	**Sieve opening, µm**	**Retained amount, %**	**Passed amount, %**	**Sieve opening, µm**	**Retained amount, %**	**Passed amount, %**
2500	3.37	96.63	1250	3.36	96.64	500	0.17	99.83	800	0.14	99.86
1250	3.34	93.29	300	8.23	88.42	300	0.78	99.05	100	3.73	96.13
500	25.12	68.17	100	19.33	69.09	150	6.26	92.79	75	5.43	90.7
300	41.57	26.6	75	5.66	63.43	100	23.28	69.51	50	10.02	80.68
100	25.18	1.42	50	11.89	51.54	75	7.21	62.3	36	23.21	57.47
50	0.53	0.89	25	24.53	27.01	36	50.09	12.21	25	31.64	25.83
25	0.04	0.85	Pan	27.01		25	10.75	1.47	Pan	25.6	
Pan	0.03	0.82				Pan	1.81				

Appendix II, 3 Sieving results of lime/$CaCO_3$ samples No. 3, 12 and 13.

Sample No. 3			Sample No. 12			Sample No. 13		
Sieve opening, µm	**Retained amount, %**	**Passed amount, %**	**Sieve opening, µm**	**Retained amount, %**	**Passed amount, %**	**Sieve opening, µm**	**Retained amount, %**	**Passed amount, %**
500	2	98	2500	16.8	83.2	300	0.03	99.97
150	83.34	14.66	800	30.48	52.73	150	0.12	99.85
100	7.09	7.57	500	31.7	21.02	100	5.18	94.67
75	2.55	5.02	100	19.75	1.27	75	6.4	88.27
50	1.63	3.39	50	0	1.27	36	36.02	52.25
25	0.05	3.34	25	0	1.27	25	43.83	8.43
Pan	0		Pan	0		Pan	8.26	

Appendix II, 4 Sieving results of lime/$CaCO_3$ and construction waste samples No. 17, 18 and 22.

Sample No. 17			Sample No. 18			Sample No. 22		
Sieve opening, µm	**Retained amount, %**	**Passed amount, %**	**Sieve opening, µm**	**Retained amount, %**	**Passed amount, %**	**Sieve opening, µm**	**Retained amount, %**	**Passed amount, %**
500	0.17	99.83	500	0.18	99.82	1250	22.87	77.13
100	43.23	56.6	150	45.33	54.49	800	10.5	66.63
75	15.18	41.43	100	29.34	25.16	500	10.93	55.70
50	16.77	24.66	75	10.25	14.9	200	26.39	29.3
36	13.2	11.46	36	10.75	4.15	75	16.15	13.15
25	8.52	2.94	25	2.26	1.89	36	5.43	7.72
Pan	2.76		Pan	2		25	6	1.72
						Pan	1.63	

APPENDIX III: PSD frequency distribution graphs of the sieved fractions. Operational parameters of Mastersizer 3000; stirrer speed of 2500 rpm, 15 s measurement duration with no ultrasonication effect. Fraunhofer optical model was applied.

Appendix III, 1 Sample 1 - Ash (bark combustion)

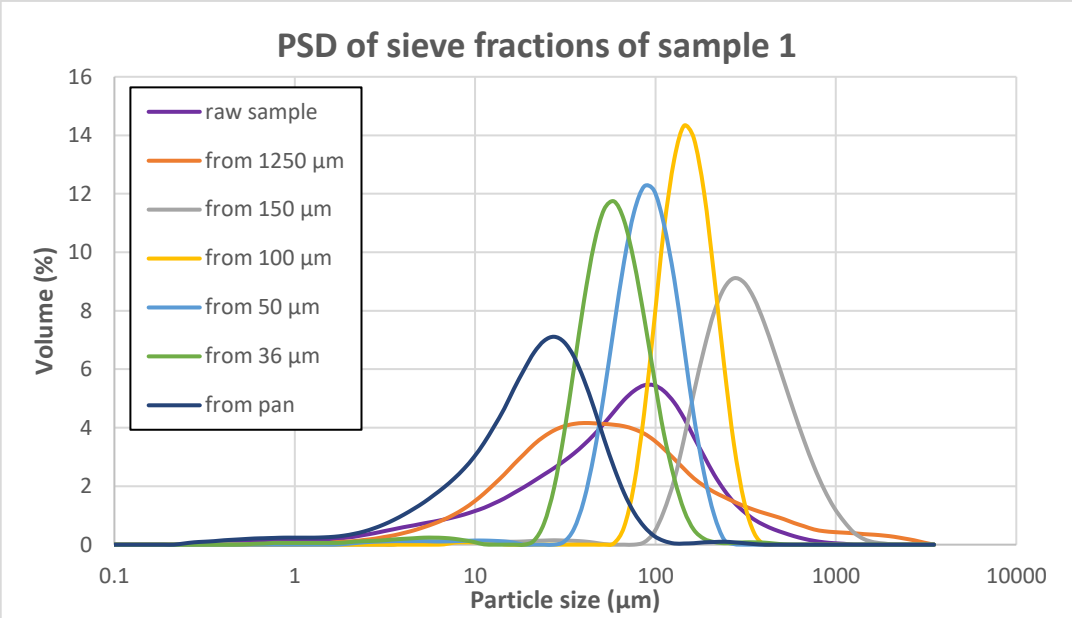

Appendix III, 2 Sample 5 - Bottom ash (co-incineration)

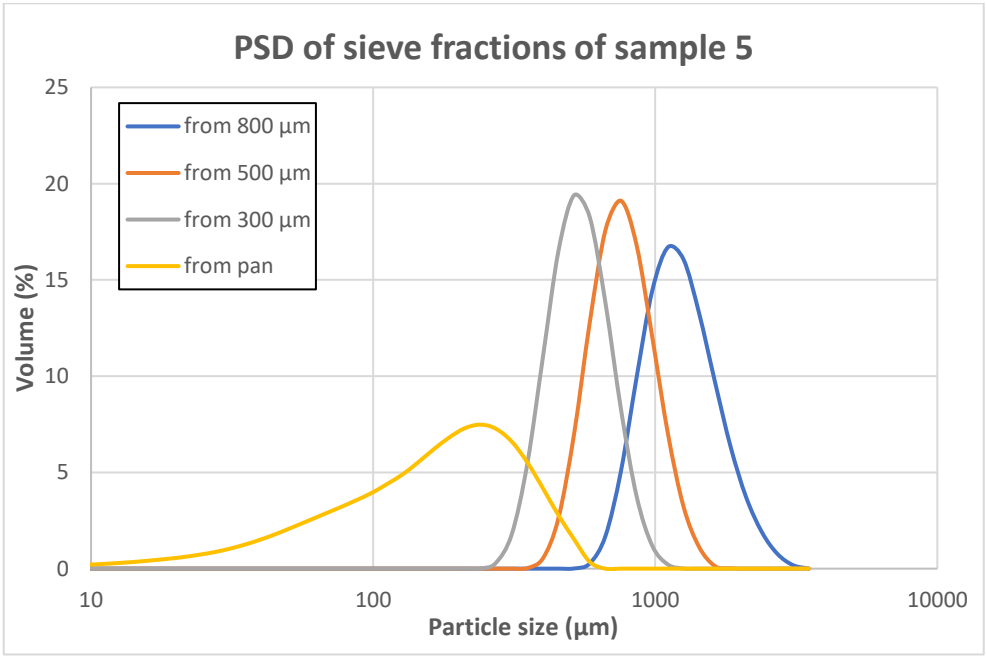

Appendix III, 3 Sample 7 - Fly ash (biomass power plant)

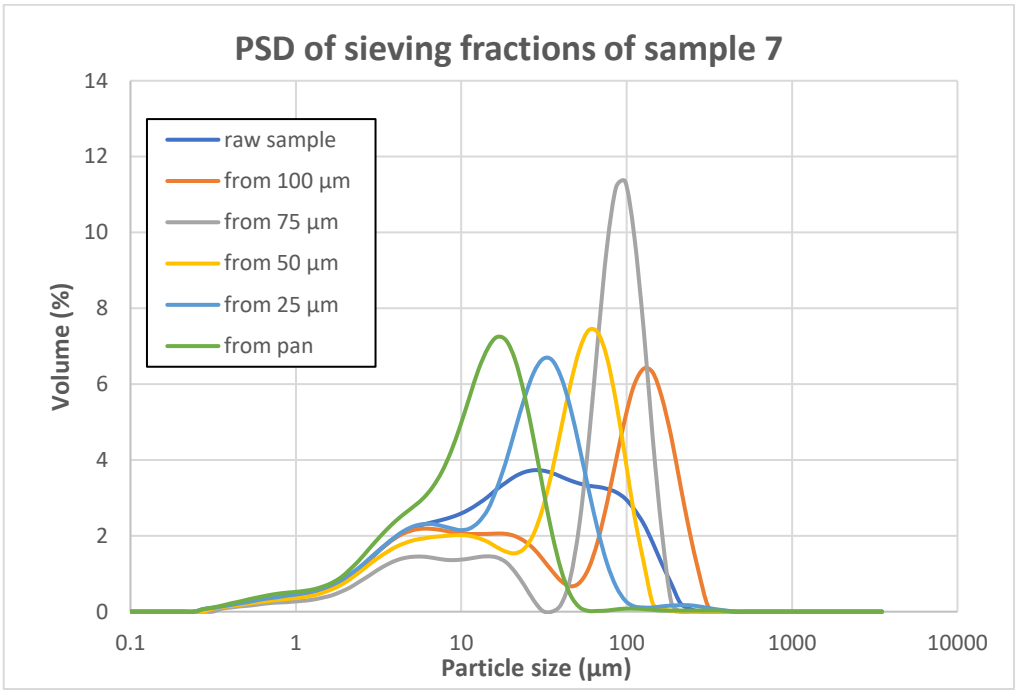

Appendix III, 4 Sample 11 - Ash (gasification of bark on $CaCO_3$ bed)

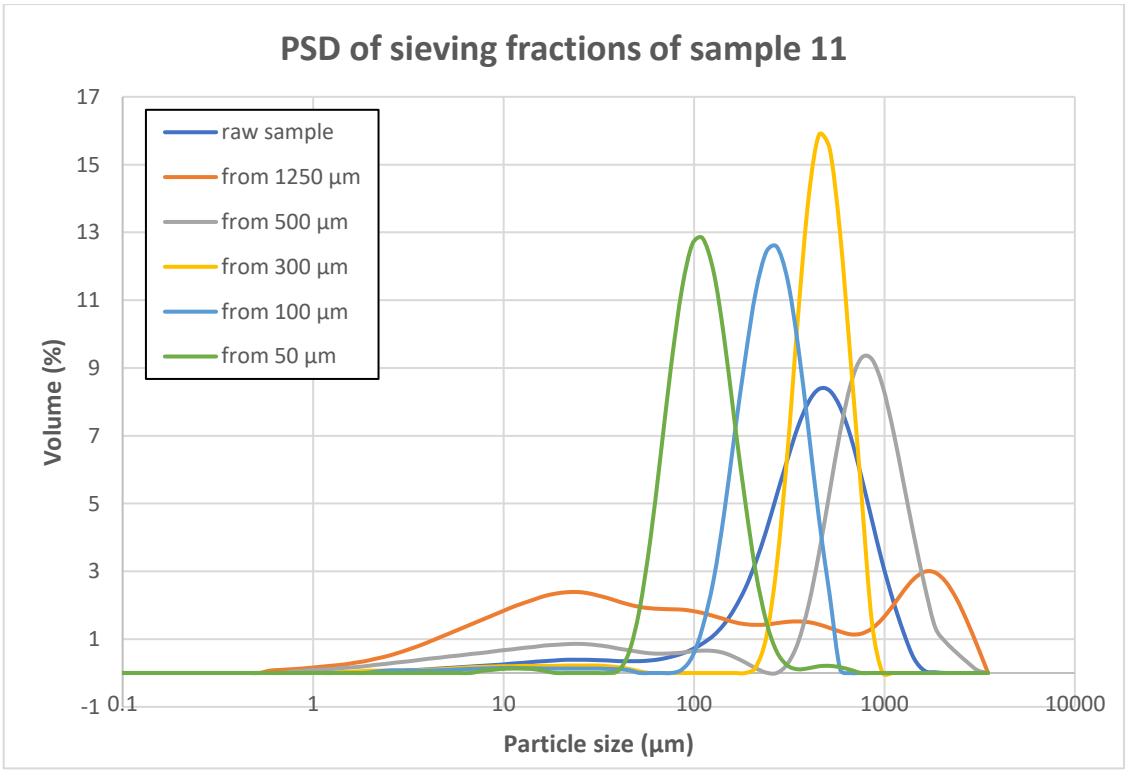

Appendix III, 5 Sample 12 - Lime/slaked lime (CaO / $Ca(OH)_2$)

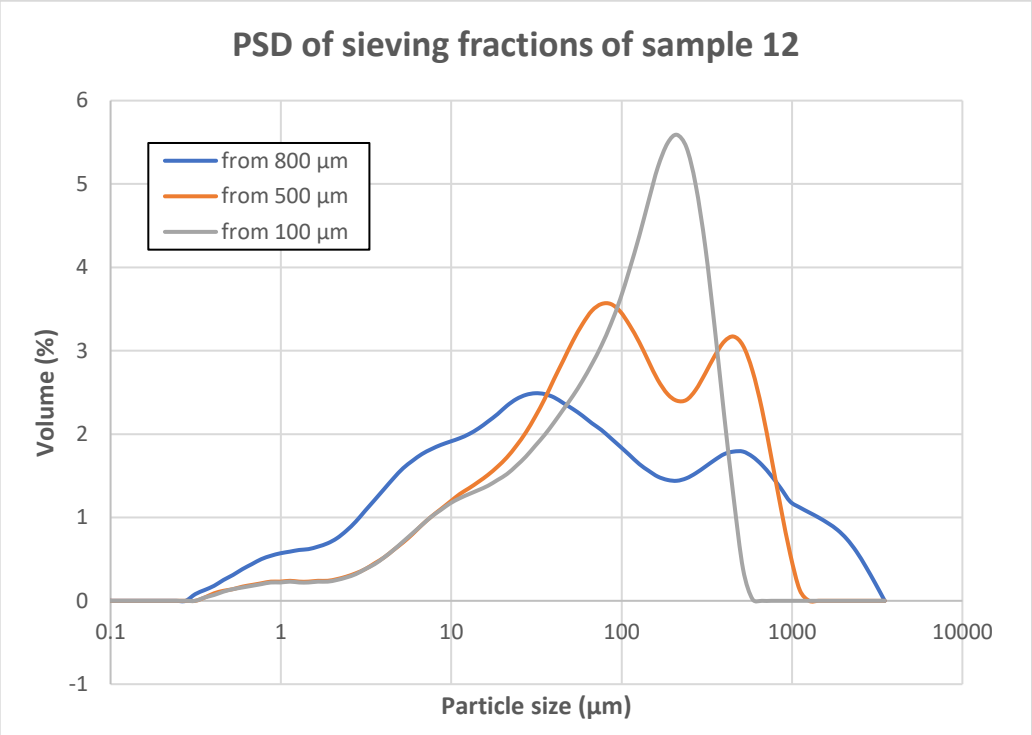

Appendix III, 6 Sample 13 - Lime kiln dust

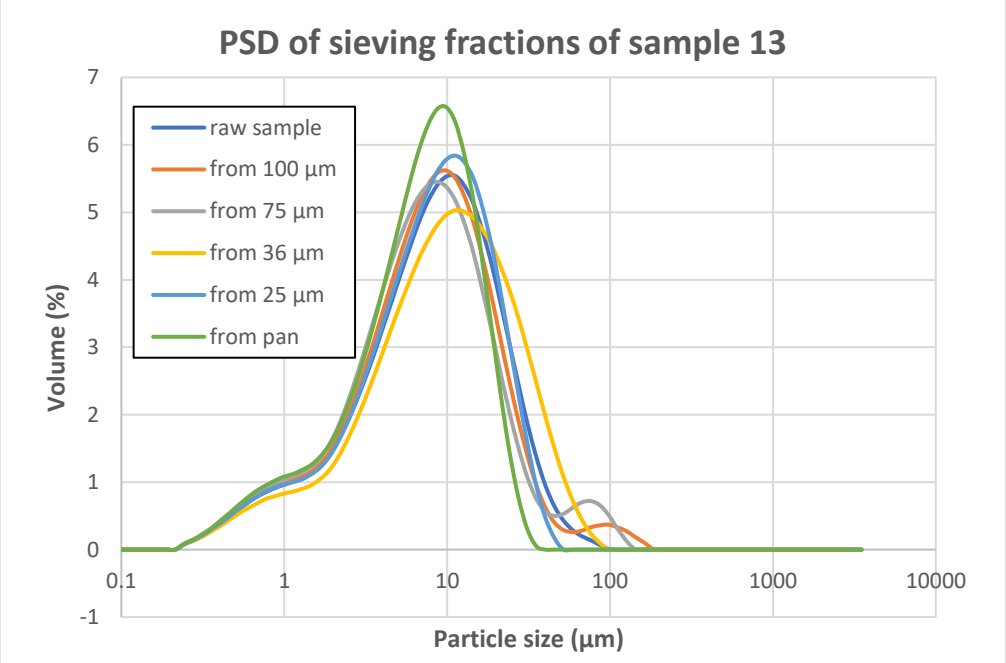

Appendix III, 7 Sample 16 - Ash (combustion of bark)

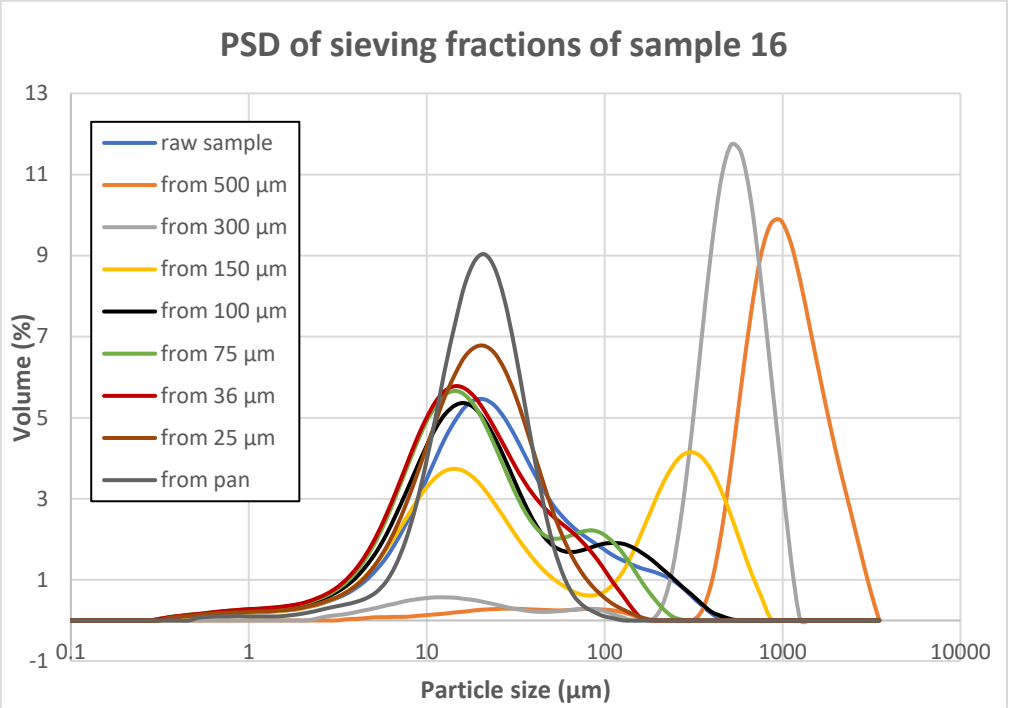

Appendix III, 8 Sample 17 - Tailings, fine fraction (from carbonate mine)

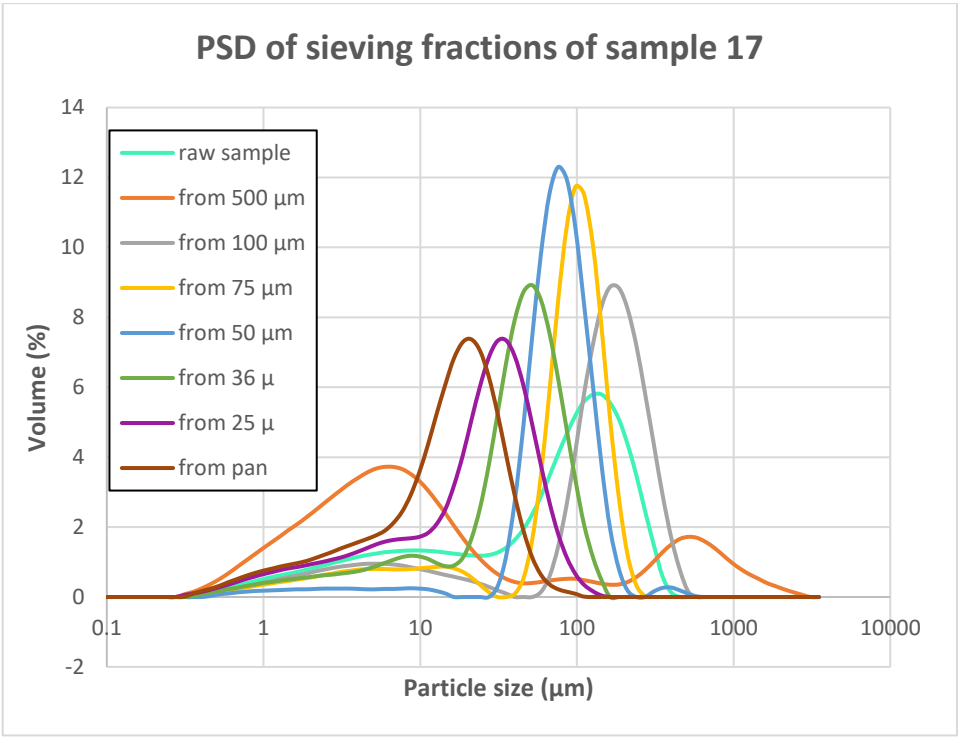

Appendix III, 9 Sample 18 - Tailings, coarse fraction (from carbonate mine)

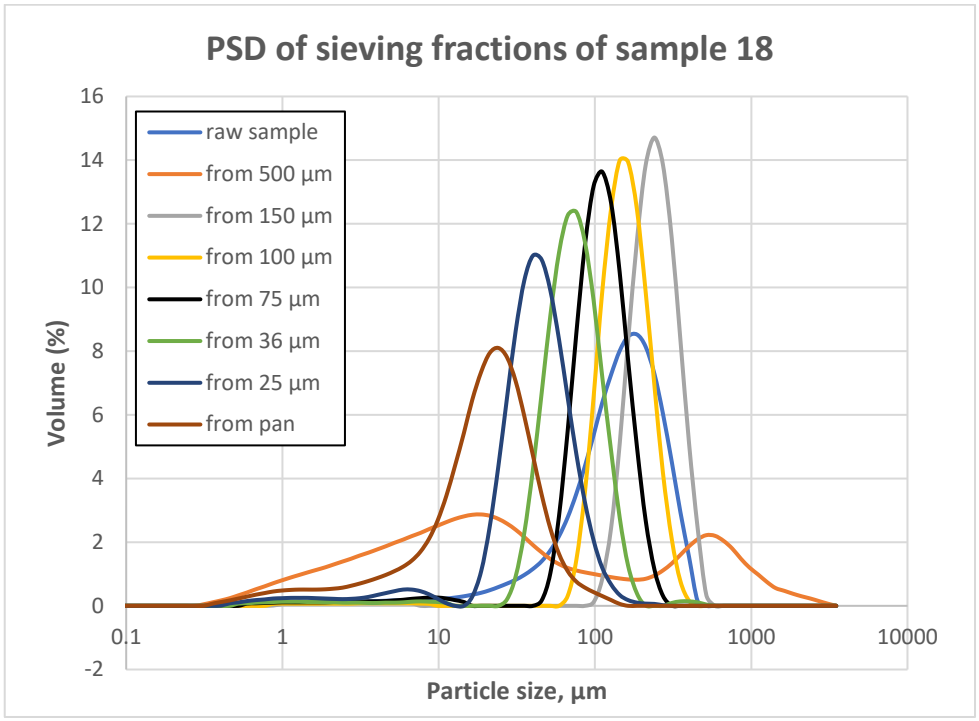

Appendix III, 10 Sample 20 - Fly ash (coal)

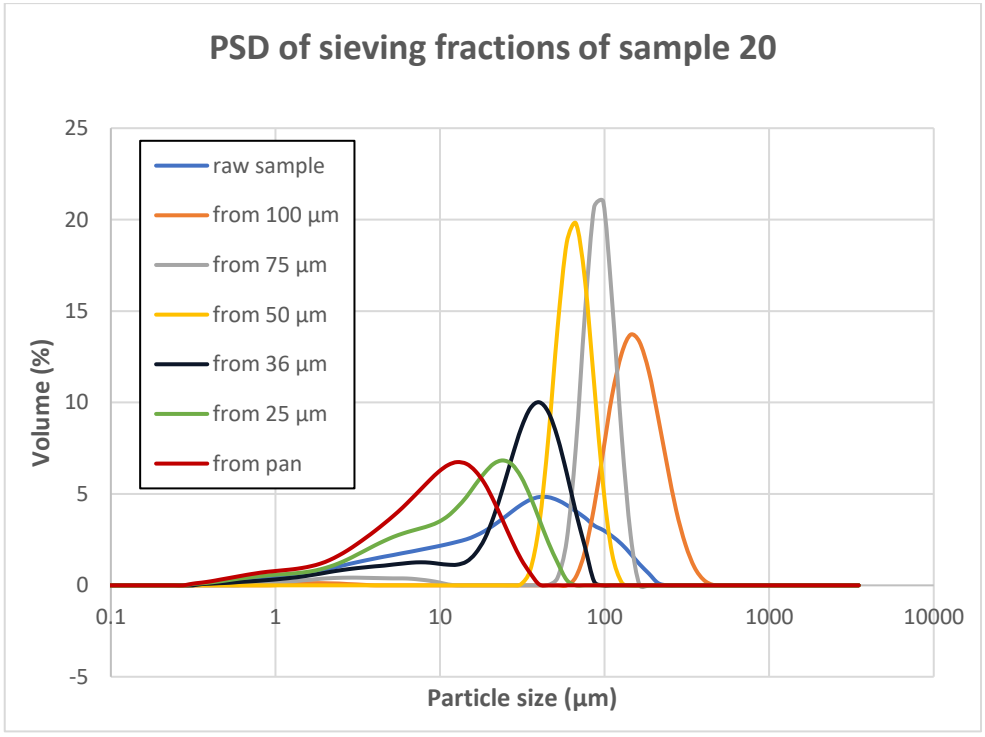

Appendix III, 11 Sample 22 - Construction waste